

Effective Models for the Anderson Impurity and the Kondo Model from Continuous Unitary Transformations

Jörn Krones^{1,*} and Götz S. Uhrig^{1,†}

¹*Lehrstuhl für Theoretische Physik I, Technische Universität Dortmund,
Otto-Hahn Straße 4, 44221 Dortmund, Germany*

(Dated: August 9, 2018)

The method of continuous unitary transformations (CUTs) is applied to the Anderson impurity and the Kondo model aiming at the systematic derivation of convergent effective models. If CUTs are applied in a conventional way, diverging differential equations occur. Similar to poor man's scaling the energy scale, below which the couplings diverge, corresponds to the Kondo temperature T_K . We present a way to apply CUTs to the Kondo and to the Anderson impurity model so that no divergences occur but a converged effective low-energy model is derived with small finite parameters at arbitrarily small energies. The ground state corresponds to a bound singlet with a binding energy given by the Kondo temperature T_K .

PACS numbers: 75.20.Hr,03.65.Ge,71.10.Pm,71.27.+a

I. INTRODUCTION

We want to apply the approach of continuous unitary transformations (CUT) to two archetypical impurity models which exhibit the *Kondo effect*, the Kondo model and the Anderson impurity model¹⁻³. The Kondo effect is one of the fundamental problems of many-body theory as it appears in a wide range of correlated electron systems, for instance in heavy-fermion systems^{3,4}, in Mott-Hubbard metal-insulators^{5,6} and in nanoscale quantum dots⁷. In such models, a wide range of energy scales is important³: from the bath electrons' bandwidth D , which can be of the order of several eV, down to the exponentially small Kondo temperature T_K .

The challenge to treat the exponentially small Kondo energy scale reliably has first been solved by the numerical renormalization group (RG)⁸⁻¹⁰. A Bethe ansatz solution put the results on a rigorous foundation¹¹.

In recent years, the issue has attracted much attention in the field of renormalization approaches. The functional RG approach was applied to the Anderson impurity model¹² yielding good results for small and intermediate interactions, but failing to reproduce the exponentially small Kondo energy scale in the strong coupling regime. Subsequently, a series of papers¹³⁻¹⁷ tried different variants of the functional RG approach to reproduce this small energy scale. While the successes in the regime of small to intermediate couplings were very interesting, the strong coupling regime eluded a description by functional RG. Only recently, Streib and co-workers provided a functional RG approach with the correct strong-coupling approach¹⁸. The additional key element in their study is to use a large magnetic field as flow parameter which is gradually lowered to zero. Furthermore, Ward identities and partial bosonization of the spin degrees of freedom are exploited.

The idea to treat the problem first at large magnetic fields where perturbation theory is perfectly well-controlled and then reducing the field gradually has been

put forward by Hewson and collaborators in a series of papers¹⁹⁻²¹. Besides this key idea they rely on perturbation theory in the renormalized effective interaction calling their approach renormalized perturbation theory (RPT). All these intensive studies performed in the last decade illustrate that the Anderson impurity model in the strong coupling regime represents a formidable methodological challenge.

In the present article, we want to show that continuous unitary transformations are also able to treat the strong coupling limit of the Anderson impurity model, i.e., the Kondo model with its exponentially small energy scale. Continuous unitary transformations exhibit an intrinsic energy separation because processes at higher energies are transformed faster than processes at lower energies. This feature is similar to standard RG approaches. The CUT approach can be set up non-perturbatively so that it is able to derive effective models even at exponentially low energies.

There are a number of applications of CUTs to the Kondo problem. Results of conventional "poor man's scaling"²² could be reproduced by a CUT in which diverging differential equations occur²³. This divergence indicates the Kondo energy scale. Another application of the CUT to the Kondo model²⁴ results in an effective model where the matrix elements of the effective interaction still exhibit logarithmic infrared divergences very similar to those found in a standard perturbative treatment¹. Furthermore, there are CUT approaches to the Kondo model which succeed in the derivation of a finite, convergent effective models. But these approaches profit from a detour via the bosonized form of the Kondo model²⁵⁻²⁷.

CUTs were also applied to the Anderson impurity model²⁸⁻³². But none of them revealed the exponential character of the Kondo temperature T_K . Nevertheless, an important previous work has been able to retrieve and to improve the Schrieffer-Wolff transformation³⁰. This approach has been extended recently to impurities which hybridize with a superconducting environment³².

In the present work, we show that CUTs yield the correct low-energy physics of the Kondo model and of the Anderson impurity model. Our approach does not rely on a bosonized reformulation. Staying in a purely fermionic description leads to convergence problems as one encounters diverging couplings²³. But we will show that a change of the reference state during the flow solves this problem avoiding the diverging couplings and yielding a finite, convergent effective low-energy model characterized by the exponentially small energy scale of the Kondo temperature.

This article is set up as follows. In the remainder of this introduction the basics of the CUTs are presented. In the next section, the Kondo model is briefly introduced and its standard treatment by means of CUTs is shown. The resulting flow equations diverge. Thus, in Sect. III a modified approach with a change of the reference state is introduced which allows us to derive a finite, well-defined effective model. This model is indeed characterized by the correct exponentially small energy scale. In Sect. IV, the Anderson impurity model is tackled by the standard CUT which again implies a diverging flow. The corresponding modified flow implying convergence is analyzed in Sect. V. Finally, the results are summarized in Sect. VI which also includes an outlook on promising future work.

A. Continuous unitary transformations

The continuous unitary transformation (CUT), also called flow equation approach, is a powerful method of theoretical quantum mechanics aiming at the systematic derivation of effective low-energy models. A CUT transforms a Hamiltonian continuously closer (or even completely) to diagonal form while connecting the transformed to the initial Hamiltonian by a unitary transformation. The method was suggested in the mid 90's³³⁻³⁵ and has been successfully applied to a wide range of problems in condensed matter physics, for a review see Ref. 36. Non-perturbative^{33,37-40} as well as perturbative^{41,42} versions have been developed in the course of the last two decades. CUTs continue to be objects of current research. Only recently, improved versions of the CUT approach have been developed: the enhanced perturbative (epCUT), the directly evaluated enhanced perturbative CUT (deepCUT)⁴³ as well as a graph-theory based version called gCUT⁴⁴.

For a CUT a continuous parameter l is introduced parametrizing the Hamiltonian

$$H(l) = U^\dagger(l) H(0) U(l). \quad (1)$$

Differentiating (1) with respect to l yields the flow equation

$$\frac{\partial H(l)}{\partial l} = [\eta(l), H(l)] \quad (2)$$

where the anti-hermitian generator

$$\eta(l) = \frac{\partial U(l)}{\partial l} U^\dagger(l) \quad (3)$$

is introduced. The flow equation (2) is the heart of the CUT approach. There are numerous ways to choose the generator^{33,38,40,42,45,46}. We will discuss later which kind of generator is employed in the present work.

Upon calculating the commutator between η and H generically operator terms will emerge which are not present in the original Hamiltonian. Their commutators have to be computed as well leading to even more terms and so on. This procedure leads to a proliferating number of emerging terms. Thus, we need to approximate at some point by truncating terms. Specifically, we employ deepCUT ideas⁴³, i.e., we will target a specific part of H and determine a system of differential equations which allows us to determine the targeted quantity correctly up to a certain order in a small expansion parameter, for instance the spin-spin interaction J or the hybridization V . We will describe the explicit procedure in the derivation of the flow equations below.

II. KONDO MODEL

First, we present our approach for the Kondo model before we will apply it to the Anderson impurity model as well. For this reason, we briefly review it here.

The Kondo model was introduced by Kondo¹ in order to explain the resistivity minimum upon lowering the temperature found in metals hosting magnetic impurities. The model describes the interaction of the conduction or bath electrons of the non-magnetic host metal with a localized spin \vec{S}_I of the impurity. The conduction electrons follow the dispersion $\epsilon_{\mathbf{k}}$. The interaction is an exchange interaction implying a spin-spin coupling J between the localized impurity spin and the spins of the bath electrons \vec{s}_b

$$H_K = \sum_{\mathbf{k},\sigma} \epsilon_{\mathbf{k}} c_{\mathbf{k}\sigma}^\dagger c_{\mathbf{k}\sigma} + J \vec{S}_I \cdot \vec{s}_b. \quad (4)$$

The Hamiltonian is given in second quantization, i.e., $c_{\mathbf{k}\sigma}^\dagger$ ($c_{\mathbf{k}\sigma}$) creates (annihilates) a bath electron with momentum \mathbf{k} and spin σ while \vec{s}_b is the bath electrons' spin

$$\vec{s}_b = \frac{1}{N} \sum_{\mathbf{k},\mathbf{k}'} \sum_{\alpha,\beta} c_{\mathbf{k}\alpha}^\dagger \vec{\sigma}_{\alpha\beta} c_{\mathbf{k}'\beta} \quad (5)$$

interacting with the local impurity spin. The components of the vector $\vec{\sigma}$ are the Pauli matrices $\vec{\sigma} = \sum_{\mu \in x,y,z} \sigma^\mu \vec{e}_\mu$ as usual.

A. Logarithmic discretization

The Hamiltonian in energy representation is simpler than the initial Hamiltonian. Let us assume that all pa-

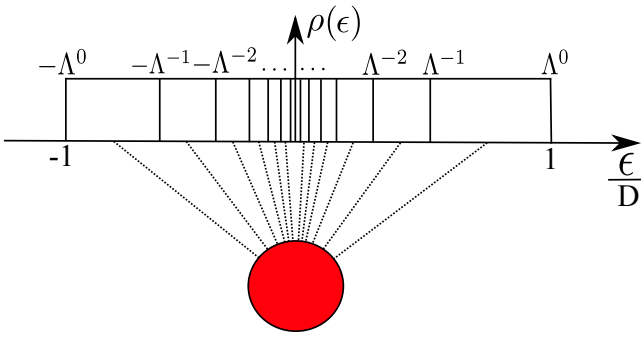


FIG. 1. (Color online) Logarithmic discretization of the continuum of the bath electrons sketched for a flat density of states (DOS) $\rho(\epsilon) = \rho_0 \Theta(D - |\omega|)$ with $\rho_0 = 1/(2D)$ and a band width $2D$ coupled to an impurity.

parameters are isotropic and thus only depend on the absolute value $|\mathbf{k}|$ of the momenta. Due to this isotropy, it is convenient to introduce spherical coordinates. Finally, a substitution $k \rightarrow \epsilon(k)$ is used. This leads to the continuum energy representation. For details of the required steps, the reader is referred to Ref. 9. Numerically, a continuum of operators or states can hardly be handled. Thus we use a logarithmic discretization of the energy representation, see, e.g., Refs. 9 and 10.

The important energies of the Kondo problem stretch from the bandwidth D down to exponentially small energies below the Kondo temperature T_K . A linear discretization is not suitable in such a problem. Thus one resorts to the logarithmic discretization sketched in Fig. 1, for details see Ref. 10. The continuum of the bath electrons is discretized in exponentially decreasing intervals

$$\frac{I_n^+}{D} = [\Lambda^{-n-1}, \Lambda^{-n}] \quad (6a)$$

$$\frac{I_n^-}{D} = [-\Lambda^{-n}, -\Lambda^{-n-1}] \quad (6b)$$

where $\Lambda > 1$ determines the discretization and $n \in \mathbb{N}$. The length of the n th interval is given by

$$\frac{d_n}{D} = (1 - \Lambda^{-1}) \Lambda^{-n}. \quad (7)$$

In this logarithmic discretization, the higher energies are only covered with low precision while small energy scales are represented with an increasingly higher resolution. More precisely, the relative precision is the same at all energies, high or low. In this way, the discretization scheme easily reaches down to exponentially small energy scales below the Kondo temperature T_K .

B. Discretization of a flat density of states

In the model (4) one discretizes the bath electrons' density of states (DOS). The formal representation is given

by

$$\epsilon_n^\pm = \frac{1}{|\gamma_n^\pm|^2} \int_{I_{n,\pm}} \epsilon \rho(\epsilon) d\epsilon \quad (8a)$$

$$|\gamma_n^\pm|^2 = \int_{I_{n,\pm}} \rho(\epsilon) d\epsilon \quad (8b)$$

where we integrate over the intervals I_n^\pm according to

$$\int_{I_{n,+}} = \int_{D\Lambda^{-n-1}}^{D\Lambda^{-n}} , \quad \int_{I_{n,-}} = \int_{-D\Lambda^{-n}}^{-D\Lambda^{-n-1}} . \quad (9)$$

Then, the discretized Hamiltonian reads

$$H_K = \sum_{n,\sigma} \epsilon_n : c_{n\sigma}^\dagger c_{n\sigma} : + \sum_{\mu} \sum_{\alpha,\beta,n,m} J_{nm} \sigma_{\alpha\beta}^\mu S_I^\mu : c_{n\alpha}^\dagger c_{m\beta} : \quad (10)$$

where

$$J_{nm} = J \gamma_n \gamma_m. \quad (11)$$

The colons denote that the operators are normal-ordered with respect to the Fermi sea of the bath electrons

$$: c_{n\alpha}^\dagger c_{m\beta} : := c_{n\alpha}^\dagger c_{m\beta} - \langle \text{FS} | c_{n\alpha}^\dagger c_{m\beta} | \text{FS} \rangle. \quad (12)$$

For a flat density of states

$$\rho(\omega) = \rho_0 \Theta(D - |\omega|) \quad , \quad \rho_0 = 1/(2D) \quad (13)$$

we can easily calculate the parameters (8a)

$$\frac{\epsilon_n^\pm}{D} = \pm \frac{1}{2} (1 + \Lambda^{-1}) \Lambda^{-n} \quad (14a)$$

$$|\gamma_n^\pm|^2 = \frac{1}{2} (1 - \Lambda^{-1}) \Lambda^{-n}. \quad (14b)$$

C. Diagonalization of the spin-spin interaction

In order to diagonalize the spin-spin interaction we introduce the generator

$$\eta = \sum_{\mu} \sum_{\alpha,\beta,n,m} \eta_{nm} \sigma_{\alpha\beta}^\mu S_I^\mu : c_{n\alpha}^\dagger c_{m\beta} : \quad (15)$$

which has the same structure as the corresponding term in the Hamiltonian (4). Specifically, we use the sign generator

$$\eta_{nm} = \text{sgn}(\epsilon_n - \epsilon_m) J_{nm}. \quad (16)$$

Without further approximations this choice of the generator would lead to an effective model in which the spin-spin interaction is diagonalized within degenerate subspaces, for a proof of this statement see Ref. 38. As soon as approximations are used, this statement does not hold true necessarily and the resulting flow equations might even diverge. Nevertheless, despite the approximations,

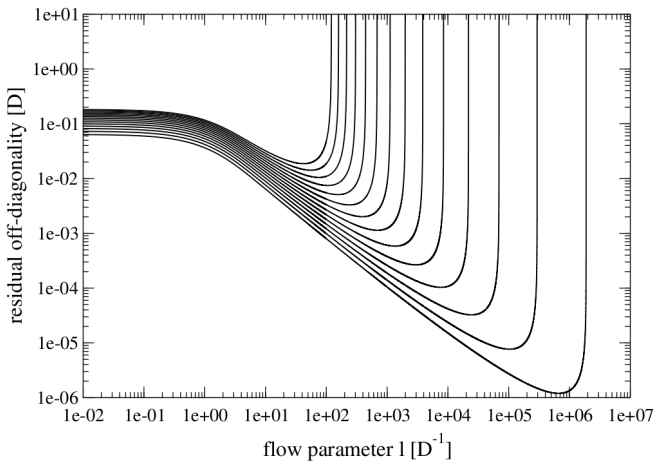


FIG. 2. (Color online) Residual off-diagonality (ROD) (20) of the flow equation (17) for the Kondo model with $N = 80$, $\Lambda = 2$ and from left to right: $2\rho_0 J = 0.2, 0.19, 0.18, \dots, 0.09, 0.08, 0.07$.

the CUT approach commonly yields sensible results if the approximations are physically justified.

Calculating the commutator between η from (15) and H_K from (10), terms emerge which so far did not appear in (10). For instance, quartic operators in the fermionic bath operators occur. We discard them *after* normal-ordering with respect to the reference state which is the Fermi sea of the fermionic bath so far. Due to the normal-ordering feedback to the spin-spin interaction in order J^2 is properly captured. Furthermore, bilinear hopping terms occur which we discard as well because they only weakly renormalize the single-particle energies ϵ_n in order J^2 . The remaining terms of the commutator are compared to the derivative of H_K leading to the flow equation (2)

$$\begin{aligned} \partial_l J_{nm} = & -|\epsilon_n - \epsilon_m| J_{nm} \\ & - \sum_x (\text{sgn}(\epsilon_n - \epsilon_x) - \text{sgn}(\epsilon_x - \epsilon_m)) (1 - 2\theta_x) J_{nx} J_{xm} \end{aligned} \quad (17)$$

where

$$\theta_x = \langle \text{FS} | c_{x\sigma}^\dagger c_{x\sigma} | \text{FS} \rangle \quad (18)$$

stems from the normal-ordering with respect to the non-interacting Fermi sea. The linear term in (17) is a generic term for a generator of the form (16). Usually, it implies exponential convergence at large l . Solving (17) numerically, however, reveals that the flow (17) diverges at some flow parameter l_0 which is related to the energy scale $T_K = l_0^{-1}$, see Figs. 2 and 3.

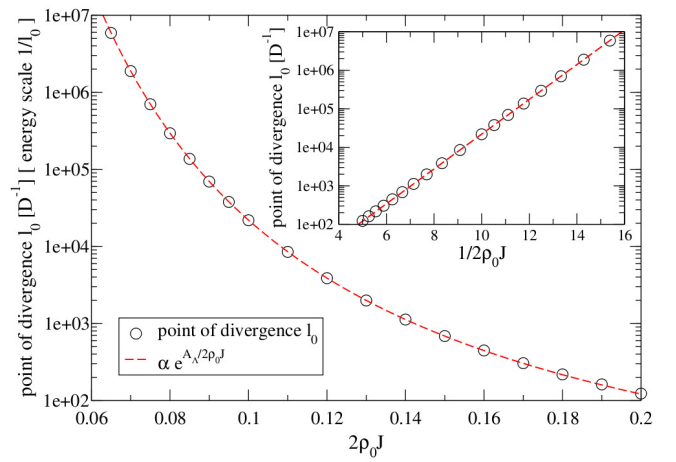


FIG. 3. (Color online) Flow parameter l_0 at which the flow equation diverges, cf. Fig. 2, for the Kondo model with $N = 80$ and $\Lambda = 2$ in a logarithmic plot vs. $2\rho_0 J$. The inset shows the exponential character $l_0 \propto \exp(A_\Lambda/2\rho_0 J)$ in a logarithmic plot as function of $1/2\rho_0 J$. The factor A_Λ is given in Eq. (22) and stems from the discretization.

D. Residual off-diagonality (ROD)

In Fig. 2 we show the residual off-diagonality (ROD) which is defined by

$$\text{ROD}^2 := \sum_{n: h_n \in \eta} |h_n|^2, \quad (19)$$

where h_n denotes the coefficients in the Hamiltonian. We sum over the square of the absolute value of all coefficients which contribute to the generator³⁸. In this way, the decrease of the ROD measures the convergence of the CUT as function of l . In the case of the flow equation (17) the ROD is given by

$$\text{ROD}^2 = \sum_{\substack{n,m \\ n \neq m}} |J_{nm}|^2. \quad (20)$$

In Fig. 2 one clearly sees that the flow first appears to converge properly, indicated by a decreasing ROD. But there is a value l_0 of the flow parameter l at which the ROD changes its behavior and rises again. It even diverges quickly beyond l_0 .

In Fig. 3 the inverse energy scale l_0 is analyzed at which the flow equation diverges. We find an exponential behavior of the form

$$l_0 = T_K^{-1} \propto e^{\frac{A_\Lambda}{2\rho_0 J}} \quad (21)$$

where the prefactor

$$A_\Lambda = \frac{1}{2} \frac{\Lambda + 1}{\Lambda - 1} \ln \Lambda \quad (22)$$

takes a well-known discretization effect⁹ into account which is independent of the applied method NRG, CUT, or others.

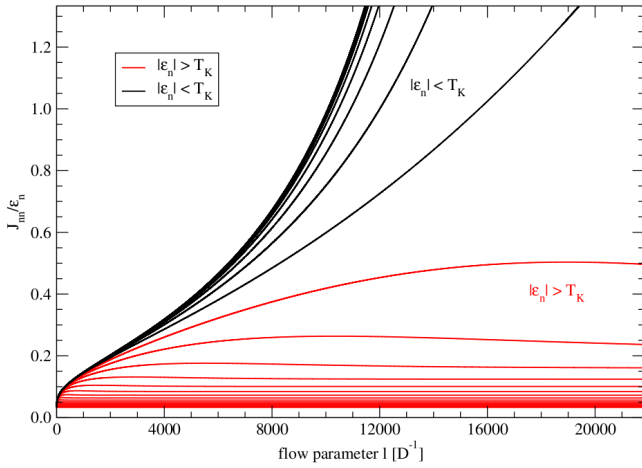


FIG. 4. (Color online) Flow of the diagonal spin-spin exchange interactions $\frac{J_{nn}(l)}{|\gamma_n|^2}$ of the Kondo model with $N = 80$, $\Lambda = 2$ and $2\rho_0 J = 0.1$. The Kondo temperature T_K is taken from the inverse of the point of divergence l_0 . The black lines show the exchange couplings with an index n for which $|\epsilon_n| < T_K$ holds while the red lines show the couplings with an index n for which $|\epsilon_n| > T_K$ holds. Note that only couplings with $|\epsilon_n| < T_K$ diverge.

This result is very similar to the outcome of Anderson's "poor man's scaling"²². The resulting differential equations diverge at the Kondo temperature T_K which we derived here in leading order in J . Truncating the flow equations in higher orders would provide higher order contributions to the Kondo temperature²³.

Fig. 4 depicts the flow of the relative exchange couplings $J_{nn}/|\gamma_n|^2$ for various values of n . Only couplings J_{nn} with an index n for which $|\epsilon_n| < T_K$ diverge in contrast to the couplings with indices corresponding to $|\epsilon_n| > T_K$ which converge towards a finite value. This observation is very interesting because it clearly shows that the spin-spin interaction only plays a dominant role *below* the Kondo energy scale. To our knowledge, it has not been derived before that only the exchange couplings to levels *below* the Kondo energy diverge while the one to levels above this scale stay finite.

III. MODIFIED APPROACH - CHANGE OF THE REFERENCE STATE DURING THE FLOW

Here we present a modification of the above approach which avoids the occurring divergences. The caveat of the above approach is the chosen reference state, i.e., the state to which the CUT aims to map the ground state. So far the ground state of the diagonal part

$$H_{D,\text{old}} = \sum_{n,\sigma} \epsilon_n c_{n\sigma}^\dagger c_{n\sigma} \quad (23)$$

was taken as the reference state leaving the spin of the impurity free. Thus the reference state is two-fold degen-

erate. Here we include the diagonal spin-spin interactions

$$H_{K,\text{diag}} = \sum_{\mu} \sum_{\alpha,\beta,n} J_{nn} \sigma_{\alpha\beta}^{\mu} S_I^{\mu} : c_{n\alpha}^\dagger c_{n\beta} : \quad (24)$$

into the diagonal Hamiltonian

$$H_{D,\text{modified}} = H_{D,\text{old}} + H_{K,\text{diag}}. \quad (25)$$

The key idea is to take the ground state of Eq. (25) as reference state. In view of the divergence of the spin-spin couplings at low energies it is indeed highly plausible, if not compulsory, that these couplings must be included in the determination of the reference state because it should be close to the true ground state. Moreover, it is known that the ground state of the Kondo model consists of a singlet state which implies that the impurity spin is correlated with a spin from the bath electrons.

In order to choose the ground state of (25) as the reference state we have to understand how it depends on the diagonal spin-spin interactions J_{nn} . In principle, it seems that we are facing a many-body problem again that is almost as difficult as the original Hamiltonian. But we can find the ground state (25) by a much simpler consideration. If the couplings J_{nn} are small enough, for instance during the early stages of the flow, the ground state is the Fermi sea. The reason is that the spin-spin interactions do not have any effect on the Fermi sea because all bath sites are either empty or doubly occupied so that there is no spin present. In order to have any effect, a spin in the bath must be created by either adding a fermion above the Fermi level or removing one from below the Fermi level. This costs energy. Then, the energy gain due to the spin-spin interaction must compensate this energy loss. This can only happen if the couplings J_{nn} are large enough relative to the energies ϵ_n .

The couplings J_{nn} increase during the flow and thus the concomitant energy gain increases compared to the energy loss. The energy balance depends on the site n and there will be one specific site where the energy balance favors the singlet formation. The other sites remain in a Fermi sea, unaffected by the spin-spin interaction.

In order to understand how the ground state changes one only has to focus on the impurity and the specific sites where it becomes energetically favorable to create a spin. We include three sites in our analysis because if the creation of a spin is favorable at the negative level $\epsilon_{\bar{r}} = -\epsilon_r$ by removing a particle then the same holds true at the positive level ϵ_r by adding a particle due to particle-hole symmetry. Thus, we consider

$$H_r = \sum_{\sigma} \epsilon_r \left(c_{r\sigma}^\dagger c_{r\sigma} - c_{\bar{r}\sigma}^\dagger c_{\bar{r}\sigma} \right) + J_{rr} \sum_{\mu} \sum_{\alpha,\beta} \sigma_{\alpha\beta}^{\mu} S_I^{\mu} \left(c_{r\alpha}^\dagger c_{r\beta} + c_{\bar{r}\alpha}^\dagger c_{\bar{r}\beta} \right) \quad (26)$$

where \bar{r} labels operators acting on the site with energy $\epsilon_{\bar{r}} = -\epsilon_r$. This problem can be solved by exact diagonalization and we find 32 eigenstates.

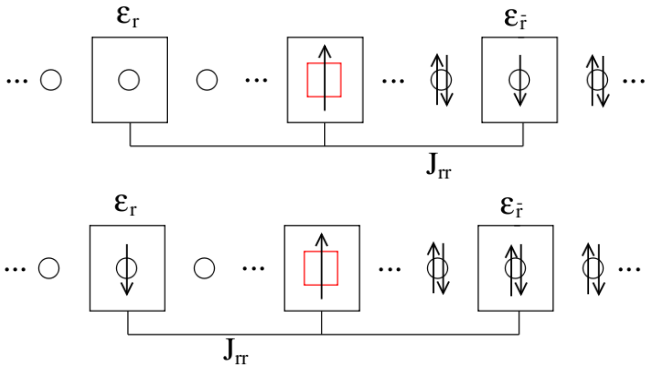


FIG. 5. (Color online) Part H_r of the Hamiltonian comprising the first sites for which it becomes energetically favorable to create a spin from the Fermi sea so that the spin-spin exchange is non-trivial. Due to particle-hole symmetry removing a particle from a negative level implies the same energy loss as adding a particle to the corresponding positive level.

In order to test the modified approach keeping the numerical calculation effort minimum, we neglect some of these eigenstates and keep the following

1. The energetically low-lying ones which are influenced by the spin-spin coupling, namely the singlet state $|s^\pm\rangle$ and the triplet states $|t_i^\pm\rangle$.
2. The Fermi sea $|\text{FS}, \sigma\rangle$ because the reference state is changed if the singlet states is lowered below the Fermi sea, i.e., these states compete to be the ground state.
3. The state $|\tilde{\sigma}\rangle$ (cf. Eq. (27)) because it may also become the ground state.

These are 12 states (cf. Eqs. (27)) out of the 32 eigenstates of the Hamiltonian (26). In essence, we neglect all states with an energy larger than the energies of the triplet states.

The modified approach does not rely on this approximation, but using the complete adapted operator basis would be less transparent and the computational effort would increase significantly. Moreover, we will see that this choice of kept states yields the expected energy scales. Nevertheless, it will be an interesting issue to implement the flow equations for the complete set of states to study the influence of the reduction of the number of kept states or to study whether an even stricter truncation is sufficient as well. In Appendix A all eigenstates of the Hamiltonian (26) are listed for completeness. The

kept states are

$$|s^-\rangle = \frac{1}{\sqrt{2}} (|0, \uparrow, \downarrow\rangle - |0, \downarrow, \uparrow\rangle) \quad (27a)$$

$$|t_1^-\rangle = |0, \uparrow, \uparrow\rangle \quad (27b)$$

$$|t_2^-\rangle = \frac{1}{\sqrt{2}} (|0, \uparrow, \downarrow\rangle + |0, \downarrow, \uparrow\rangle) \quad (27c)$$

$$|t_3^-\rangle = |0, \downarrow, \downarrow\rangle \quad (27d)$$

$$|s^+\rangle = \frac{1}{\sqrt{2}} (|\downarrow, \uparrow, \uparrow\downarrow\rangle - |\uparrow, \downarrow, \uparrow\downarrow\rangle) \quad (27e)$$

$$|t_1^+\rangle = |\uparrow, \uparrow, \uparrow\downarrow\rangle \quad (27f)$$

$$|t_2^+\rangle = \frac{1}{\sqrt{2}} (|\downarrow, \uparrow, \uparrow\downarrow\rangle + |\uparrow, \downarrow, \uparrow\downarrow\rangle) \quad (27g)$$

$$|t_3^+\rangle = |\downarrow, \downarrow, \uparrow\downarrow\rangle. \quad (27h)$$

$$|\text{FS}, \uparrow\rangle = |0, \uparrow, \uparrow\downarrow\rangle \quad (27i)$$

$$|\text{FS}, \downarrow\rangle = |0, \downarrow, \uparrow\downarrow\rangle \quad (27j)$$

$$|\tilde{\uparrow}\rangle = \frac{1}{\sqrt{6}} [|\uparrow, \uparrow, \downarrow\rangle - 2|\uparrow, \downarrow, \uparrow\rangle + |\downarrow, \uparrow, \uparrow\rangle] \quad (27k)$$

$$|\tilde{\downarrow}\rangle = \frac{1}{\sqrt{6}} [|\downarrow, \downarrow, \uparrow\rangle - 2|\downarrow, \uparrow, \downarrow\rangle + |\uparrow, \downarrow, \downarrow\rangle]. \quad (27l)$$

The notation encodes the states $|r, d, \bar{r}\rangle$ where r represents the state of positive level, \bar{r} the corresponding state at the negative level and d the state of the impurity. The states $|s^-\rangle$ and $|t_i^-\rangle$ refer to the singlet and triplet states formed with the negative level at $\epsilon_{\bar{r}} = -\epsilon_r$ while the states $|s^+\rangle$ and $|t_i^+\rangle$ refer to the singlet and triplet states formed with the positive level at ϵ_r . The states $|\text{FS}, \sigma\rangle$ are the Fermi sea and a spin σ at the impurity while the states $|\tilde{\sigma}\rangle$ refer to a state with an effective spin $\frac{1}{2}$.

The eigenvalues of the states in Eq. (27) read

$$E_{s^\pm} = -\frac{3J_{rr}}{2} - \epsilon_r, \quad E_{t_i^\pm} = \frac{J_{rr}}{2} - \epsilon_r \quad (28a)$$

$$E_{\text{FS}, \sigma} = -2\epsilon_r, \quad E_{\tilde{\sigma}} = -2J_{rr}. \quad (28b)$$

The indices s^\pm and t_i^\pm refer to the singlet and triplet states formed with the negative level at $\epsilon_{\bar{r}} = -\epsilon_r$ and the positive level at ϵ_r in Eq. (27) while the indices FS, σ refer to the Fermi sea and $\tilde{\sigma}$ to the states with effective spin $\frac{1}{2}$ in Eq. (27).

The parameter regimes with their respective ground states are given by

$$J_{rr} < \frac{2\epsilon_r}{3} \quad \text{ground state: } |\text{FS}, \sigma\rangle \quad (29a)$$

$$\frac{2\epsilon_r}{3} < J_{rr} < 2\epsilon_r \quad \text{ground state: } |s^\pm\rangle \quad (29b)$$

$$J_{rr} > 2\epsilon_r \quad \text{ground state: } |\tilde{\sigma}\rangle. \quad (29c)$$

As soon as the point

$$J_{rr}(l_0) = \frac{2\epsilon_r}{3} \quad (30)$$

is reached the ground state switches from the Fermi sea to the singlet state. To be precise, both of them are doubly

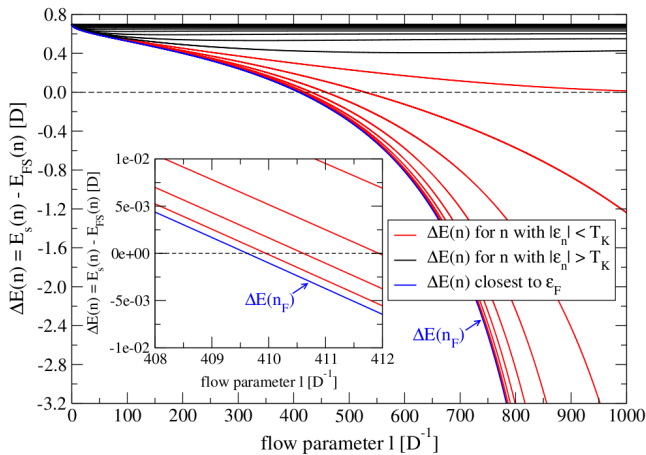


FIG. 6. (Color online) Energy difference between the singlet state and the Fermi sea $\Delta E(n) = E_s(n) - E_{\text{FS}}(n)$ at site n from (28) for the Kondo model with $N = 40$, $\Lambda = 2$ and $2\rho_0 J = 0.14$. The sites n belong to the negative energy levels and the absolute values of the energies are decreasing from top to bottom. The Kondo temperature T_K is taken from the inverse flow parameter l_0 where the flow starts to diverge. The black lines mark the flow for the n for which $|\epsilon_n| < T_K$ while the red lines mark the flow for the n for which $|\epsilon_n| > T_K$. At the value of l where one $\Delta E(n)$ vanishes the reference state is changed. The blue line shows $\Delta E(n_F)$ at the site closest to the Fermi level. The inset shows that the site closest to the Fermi level forms the singlet first.

degenerate because the singlet can be formed with site r or \bar{r} due to particle-hole symmetry. The singlet states are no Slater determinants and thus Wick's theorem cannot be applied. But the remaining bath, of course, remains a Slater determinant and Wick's theorem and the usual normal-ordering can be used as before.

At the point where the singlet states become energetically favorable, we choose the singlet states as the reference states and the states (27) as a new basis. This means that first, we solve the flow (17) in the conventional operator basis with the starting values (11). We track the ratio J_{nn}/ϵ_n at each site and as soon as the ratio reaches $2/3$ for some n we change the reference state.

Fig. 6 depicts the energy difference

$$\Delta E(n) = E_s(n) - E_{\text{FS}}(n) \quad (31)$$

between the energy of the singlet state E_s and the energy of the Fermi sea E_{FS} at a site n for the Kondo model. At the first value of l where this difference vanishes, the reference state is changed. The couplings J_{nn} only diverge for indices n with $|\epsilon_n| < T_K$ (cf. Fig. 4), i.e., only couplings below the Kondo energy scale become large enough to make a change of reference state possible. Thus, the approach ensures intrinsically that the singlet will form below the Kondo energy scale. The results displayed in Fig. 4 show that the smaller the energy ϵ_n , the faster the ratio J_{nn}/ϵ_n increases. Thus, the singlet forms at the lowest energy scale in the system. In

a continuum of states this would be infinitesimally close to the Fermi level ϵ_F . In the logarithmically discretized numerical treatment this is the bath site with the lowest energy.

Once we changed the reference state we compute the flow as discussed below in a modified operator basis. We do not allow for further changes of the reference state which may occur in principle. But we will show below that the chosen switched reference state ensures a convergent flow. To achieve convergence is the primary goal of our present study. In addition, the singlet reference states acquire a binding energy equal to the Kondo energy scale in the course of the flow. Thus there is no indication of a need to change the reference state further. Moreover, each change of reference state is cumbersome to implement so that we have to leave a comprehensive discussion of this point to future research.

A. Effective model and the modified operator basis

In the next step we determine the effective Hamiltonian and the modified flow equations due to the changed reference state. We denote the site which is part of the modified operator basis by r and the flow parameter at which the reference state is changed by l_0 . When the flow parameter reaches the point $l = l_1$, the effective Hamiltonian is still of the form

$$H(l_1) = \sum_{n,\sigma} \epsilon_n : c_{n\sigma}^\dagger c_{n\sigma} : + \sum_{\mu} \sum_{n,m} \sum_{\alpha,\beta} J_{nm}(l_1) \sigma_{\alpha\beta}^\mu S_I^\mu : c_{n\alpha}^\dagger c_{m\beta} : . \quad (32)$$

The sites denoted by r and \bar{r} , where $\epsilon_{\bar{r}} = -\epsilon_r$, form the singlet state with the impurity. Thus we treat them separately. Next we introduce the modified operator basis pertaining to these three sites which is adapted to the changed reference state

$$\hat{O}_{kq} = |k\rangle\langle q| - \langle \hat{O}_{kq} \rangle \quad (33)$$

where k and q denote the basis states from (27). The subtraction of the expectation values stands for normal-ordering. Because the states $|s^- \rangle$ and $|s^+ \rangle$ are degenerate we cannot use a single reference state but a reference ensemble⁴⁷

$$\langle \hat{O} \rangle = \frac{1}{2} \left(\langle s^- | \hat{O} | s^- \rangle + \langle s^+ | \hat{O} | s^+ \rangle \right). \quad (34)$$

The operator basis from (33) is normal-ordered with respect to this reference ensemble. Due to the normal-ordering (33), hopping terms will generically emerge in the course of the flow which eventually change the energies E_k . But all effects on E_k stemming from the normal-ordering are at least of order J^3 because all terms arising in this way are of order J^2 and they need at least one more commutation to act on E_k which increases the order in powers of J at least by one. We focus on orders up

to J^2 in the local energies and thus neglect the normal-ordering from (33) using $\hat{O}_{kq} = |k\rangle\langle q|$ instead.

We expand all terms in the modified operator basis yielding the Hamiltonian in the form

$$\begin{aligned} \bar{H}(l_0) &= \sum_{n \neq \pm r, \sigma} \epsilon_n : c_{n\sigma}^\dagger c_{n\sigma} : + \sum_{k,q} E_{kq} |k\rangle\langle q| \\ &+ \sum_{k,q} \sum_{n,m \neq \pm r} \sum_{\alpha,\beta} J_{nm}^{kq\alpha\beta} |k\rangle\langle q| : c_{n\alpha}^\dagger c_{m\beta} : \\ &+ \sum_{k,q,\sigma} \sum_{n \neq \pm r} \Gamma_n^{kq\sigma} (|k\rangle\langle q| c_{n\sigma} + c_{n\sigma}^\dagger |q\rangle\langle k|). \end{aligned} \quad (35)$$

The basis states and the modified operators were chosen such that terms acting only on the sites r or \bar{r} are diagonal. Hence we know by construction that the E_k are given by the eigenvalues in (28) where $J_{rr} = J_{rr}(l_1)$ while the starting values for the other coefficients are determined from

$$J_{nm}^{kq\alpha\beta}(l_1) = J_{nm}(l_1) \sum_{\mu} \sigma_{\alpha\beta}^\mu \langle k | S_I^\mu | q \rangle \quad (36a)$$

$$\begin{aligned} \Gamma_n^{kq\sigma}(l_1) &= J_{nr}(l_1) \sum_{\mu,\alpha} \sigma_{\alpha\sigma}^\mu \langle k | S_I^\mu c_{r\alpha}^\dagger | q \rangle \\ &+ J_{n\bar{r}}(l_1) \sum_{\mu,\alpha} \sigma_{\alpha\sigma}^\mu \langle k | S_I^\mu c_{\bar{r}\alpha}^\dagger | q \rangle \end{aligned} \quad (36b)$$

$$E_{kq}(l_1) = 2\Re \left(\sum_{\mu} \sum_{\alpha,\beta} J_{r\bar{r}} \sigma_{\alpha\beta}^\mu \langle k | S_I^\mu c_{\bar{r}\alpha}^\dagger c_{r\beta} | q \rangle \right) \quad (36c)$$

The structure of the generator after changing the reference ensemble is given by

$$\begin{aligned} \eta &= \sum_{k,q} \sum_{\alpha,\beta} \sum_{n,m \neq \pm r} \eta_{nm,J}^{kq\alpha\beta} |k\rangle\langle q| : c_{n\alpha}^\dagger c_{m\beta} : \\ &+ \sum_{k,q,\sigma} \sum_{n \neq \pm r} \eta_{n,\Gamma}^{kq\sigma} (|k\rangle\langle q| c_{n\sigma} - \text{h.c.}) + \sum_{k,q} \eta_{kq}^E |k\rangle\langle q|. \end{aligned} \quad (37)$$

We want to eliminate all terms that couple to the reference ensemble. Thus we choose the coefficients of the generator of the form

$$\eta_{kq}^E = \begin{cases} \text{sgn}(E_k - E_q) E_{kq} & \text{if } k, q = s^\pm \\ 0 & \text{otherwise} \end{cases} \quad (38a)$$

$$\eta_{nm,J}^{kq\alpha\beta} = \begin{cases} \text{sgn}(E_k - E_q + \epsilon_n - \epsilon_m) J_{nm}^{kq\alpha\beta} & \text{if } k, q = s^\pm \\ 0 & \text{otherwise} \end{cases} \quad (38b)$$

$$\eta_{n,\Gamma}^{kq\sigma} = \begin{cases} \text{sgn}(E_k - E_q - \epsilon_n) \Gamma_n^{kq\sigma} & \text{if } k, q = s^\pm \\ 0 & \text{otherwise} \end{cases}, \quad (38c)$$

where $k, q = s^\pm$ means that k or q are in one of the singlet states.

Summarizing, we only include terms which couple to the singlet states. We emphasize that this implies that terms which couple to the triplet states formed from the impurity spin and a spin on a bath site at the Fermi level are not eliminated because they are not included in the generator. Thus, the reference state, which becomes the ground state in the course of the flow, consists of a

singlet and a Fermi sea. But this does not imply that the complete effective model is reduced to a singlet and a free fermionic bath. This fact makes an exhaustive analysis of the effective model challenging.

In order to obtain the modified flow equation (2), we commute the generator (37) with the Hamiltonian (35). We truncate terms which have a quartic structure in the fermionic bath operators. The resulting flow equation reads

$$\begin{aligned} \partial_l E_{kq} &= (E_{qq} - E_{kk}) \eta_{kq}^E + \sum_{p \neq q} \eta_{kp}^E E_{pq} - \sum_{p \neq k} \eta_{pq}^E E_{kp} \\ &+ \sum_p \sum_{\alpha,\beta} \sum_{n,m \neq \pm r} \eta_{nm,J}^{kp\alpha\beta} J_{mn}^{pq\beta\alpha} \theta_n (1 - \theta_m) \\ &- \sum_p \sum_{\alpha,\beta} \sum_{n,m \neq \pm r} \eta_{mn,J}^{pq\alpha\beta} J_{nm}^{kp\beta\alpha} \theta_n (1 - \theta_m) \\ &- \sum_{n \neq \pm r} \sum_{p,\gamma} \left(\eta_{n,\Gamma}^{pk\gamma} \Gamma_n^{pq\gamma} + \eta_{n,\Gamma}^{pq\gamma} \Gamma_n^{pk\gamma} \right) \theta_n \\ &+ \sum_{n \neq \pm r} \sum_{p,\gamma} \left(\eta_{n,\Gamma}^{kp\gamma} \Gamma_n^{qp\gamma} + \eta_{n,\Gamma}^{qp\gamma} \Gamma_n^{kp\gamma} \right) (1 - \theta_n) \end{aligned} \quad (39a)$$

$$\begin{aligned} \partial_l \Gamma_n^{kq\sigma} &= (\epsilon_n + E_{qq} - E_{kk}) \eta_{n,\Gamma}^{kq\sigma} \\ &+ \sum_{p \neq q} \left(\eta_{n,\Gamma}^{kp\sigma} E_{pq} - \eta_{pq}^E \Gamma_n^{kp\sigma} \right) \\ &- \sum_{p \neq k} \left(\eta_{n,\Gamma}^{pq\sigma} E_{kp} - \eta_{kp}^E \Gamma_n^{pq\sigma} \right) \\ &+ \sum_p \sum_{x \neq \pm r, \gamma} \left(\eta_{x,\Gamma}^{kp\gamma} J_{xn}^{pq\gamma\sigma} - \eta_{xn,J}^{pq\gamma} \Gamma_x^{kp\gamma} \right) (1 - \theta_x) \\ &+ \sum_p \sum_{x \neq \pm r, \gamma} \left(\eta_{x,\Gamma}^{pq\gamma} J_{xn}^{kp\gamma\sigma} - \eta_{xn,J}^{kp\gamma} \Gamma_x^{pq\gamma} \right) \theta_x \end{aligned} \quad (39b)$$

$$\begin{aligned} \partial_l J_{nm}^{kq\alpha\beta} &= (\epsilon_m - \epsilon_n + E_{qq} - E_{kk}) \eta_{nm,J}^{kq\alpha\beta} \\ &+ \sum_{p \neq q} \left(\eta_{nm,J}^{kp\alpha\beta} E_{pq} - \eta_{pq}^E J_{nm}^{kp\alpha\beta} \right) \\ &- \sum_{p \neq k} \left(\eta_{nm,J}^{pq\alpha\beta} E_{kp} - \eta_{kp}^E J_{nm}^{pq\alpha\beta} \right) \\ &+ \sum_{x \neq \pm r, \gamma, p} \left(\eta_{nx,J}^{pq\alpha\gamma} J_{xm,J}^{kp\gamma\beta} - \eta_{xm,J}^{kp\gamma\beta} J_{nx}^{pq\alpha\gamma} \right) \theta_x \\ &+ \sum_{x \neq \pm r, \gamma, p} \left(\eta_{nx,J}^{kp\alpha\gamma} J_{xm,J}^{pq\gamma\beta} - \eta_{xm,J}^{pq\gamma\beta} J_{nx}^{kp\alpha\gamma} \right) (1 - \theta_x) \\ &- \sum_p \left(\eta_{n,\Gamma}^{pk\alpha} \Gamma_m^{pq\beta} + \eta_{m,\Gamma}^{pq\beta} \Gamma_n^{pk\alpha} \right) \\ &- \sum_p \left(\eta_{n,\Gamma}^{qp\alpha} \Gamma_m^{kp\beta} + \eta_{m,\Gamma}^{kp\beta} \Gamma_n^{qp\alpha} \right). \end{aligned} \quad (39c)$$

where $\Theta_x := \langle c_{x\sigma}^\dagger c_{x\sigma} \rangle$ is the expectation value with respect to the Fermi sea. It occurs upon the normal-ordering of the fermionic bath operators with respect to the Fermi sea.

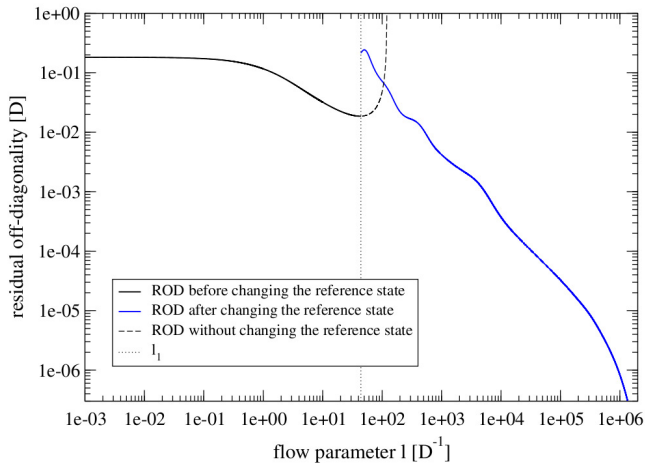


FIG. 7. (Color online) ROD for the Kondo model with $N = 40$, $\Lambda = 2$ and $2\rho_0 J = 0.2$ obtained from the modified approach where the reference state is changed during the flow at l_1 . First, the Fermi sea is the reference state and (17) is solved with the initial values (11). After changing the reference state the modified flow (39) is solved. The modified flow converges in contrast to the original CUT. The ROD for the original CUT (17) without changing the reference state is denoted by the dashed line.

B. Results of the modified flow

The number of indices is very large and one should reduce the number of differential equations by exploiting symmetries. A lot of combinations of the k and q indices, for instance, do not occur due to spin conservation which reduces the numerical effort. In the following paragraphs the results obtained by the modified approach are presented. Fig. 7 depicts the ROD of the Kondo model in the modified approach. The aim is to verify that the flow (39) converges.

We start from the Kondo Hamiltonian and solve the original flow (17) with the initial values (11). This implies that the Fermi sea is the reference state. For small l the ratio J_{nn}/ϵ_n is significantly smaller than $2/3$, cf. (30), and the flow proceeds as long as this holds true. At some value l_1 the spin-spin coupling J_{nn} becomes large enough so that $J_{nn}/\epsilon_n = 2/3$ is fulfilled. As soon as this happens, we change the reference state and rewrite the Hamiltonian in the form (35) with the modified operator basis (27). Then, we use the modified flow (39) and continue with the flow starting at l_1 . All sets of differential equations are solved by a 4th-order Runge-Kutta algorithm.

For small l the ROD is the same as for the original flow (17) because the reference state is not changed yet. Once we switch to the modified reference state, the ROD changes discontinuously because the generator is changed so that other types of terms are included in the ROD. One may wonder why the ROD increases upon changing the reference state although we aim at eliminating less terms

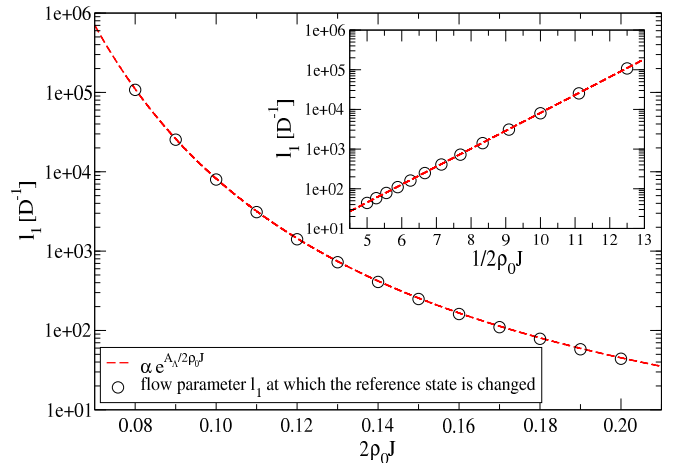


FIG. 8. (Color online) Inverse energy scale l_1 at which the reference state is changed for the Kondo model with $\Lambda = 2$ and $N = 52$. The inverse energy scale l_1 is increasing proportionally to the inverse of the Kondo temperature $T_K^{-1} \propto \exp(A_\Lambda/2\rho_0 J)$. The factor A_Λ from (22) is due to the discretization.

than before. Recall that we only rotate away terms that couple to the singlet states. But one must also bear in mind that we include completely different types of terms in the generator after the change to the modified operator basis. In particular, terms that are diagonal in the fermionic bath operators are then included which were not included before. For instance, we may inspect terms of the form

$$J_{nn}^{t_i^\pm, s^\pm, \alpha\beta} |t_i^\pm\rangle \langle s^\pm| : c_{n\alpha}^\dagger c_{n\beta} : \quad (40)$$

with initial values at l_1 that are proportional to $J_{nn}(l_1)$. Such terms were not eliminated by the CUT in the conventional, original operator basis. Thus, at $l = l_1$ these terms are large compared to the terms in the generator before the reference state is changed which have been suppressed by a factor $\exp(-|\epsilon_n - \epsilon_m|l_1)$. Once the reference state is changed, these diagonal terms in the fermionic bath operators are included in the ROD. Thus, the ROD increases abruptly upon switching the reference state and using the modified generator.

The dashed line in Fig. 7 shows the behavior of the ROD if the reference state is not changed. In this case the ROD diverges at l_0^{-1} corresponding to the Kondo temperature T_K . We conclude that the modified flow equation (39) is indeed able to prevent this divergence leading to an effective Hamiltonian with finite couplings even at the Fermi level $\epsilon_F = 0$.

We succeeded to provide a method that yields an effective Hamiltonian with small finite parameters for $\epsilon \rightarrow \epsilon_F$. With the conventional, original approach we found the Kondo energy scale only as the point at which the running couplings diverge²³. Fig. 8 depicts the inverse energy scale given by the flow parameter l_1 at which the reference state is changed for the Kondo model. We re-

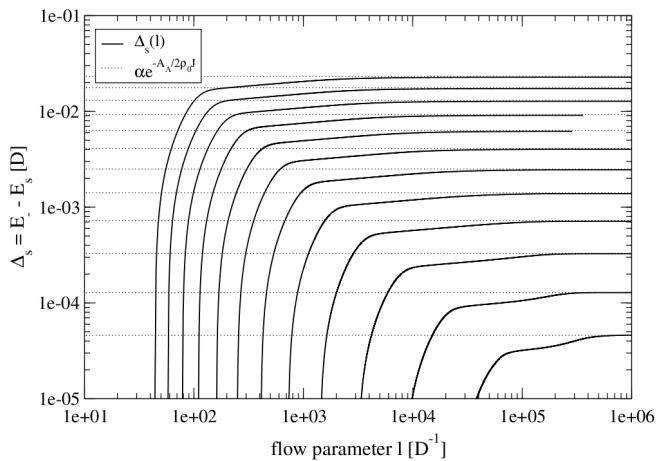


FIG. 9. (Color online) Flow of $\Delta_s(l) = E_-(l) - E_s(l)$ with E_- and E_s from (45a) for the Kondo model with $N = 40$ and $\Lambda = 2$. The quantity Δ_s converges to the binding energy of the Kondo singlet for $l \rightarrow \infty$.

trieve the exponential energy scale

$$l_1^{-1} \propto e^{-\frac{A_\Lambda}{2\rho_0 J}} \quad (41)$$

where the factor A_Λ is given by (22) taking discretization effects into account⁹. Thus, we confirm that the energy scale at which the reference state is changed is proportional to the Kondo temperature T_K , at least at the level of accuracy of the present study.

In addition, there is another very interesting energy scale in the effective model which is the *binding energy* of the singlets. This energy is the energy by which the singlets are separated from the Fermi sea states with a localized spin on the impurity. Note that this does not imply that the system is gapped because the other fermionic sites still exist and represent massless excitations in the continuum limit.

We can identify the local binding energy easily as the energy difference Δ_s of the two lowest energies E_s and E_- in the diagonal part (45a) of the Hamiltonian (44) where the E_{kq} are diagonalized first, cf. also (28). Hence we consider

$$\Delta_s = E_- - E_s \quad (42)$$

at $l \rightarrow \infty$.

If we omit the remaining interactions at finite l , we can define an approximative binding energy of the singlet state by the energy difference between the two lowest energy levels

$$\Delta_s(l) = E_-(l) - E_s(l) \quad (43)$$

from the effective Hamiltonian

$$H_{\text{eff}} = \sum_{n,\sigma} \epsilon_n : c_{n\sigma}^\dagger c_{n\sigma} : + \sum_k E_{kk} |k\rangle \langle k| + g \sum_\sigma (|FS, \sigma\rangle \langle \tilde{\sigma}| + |\tilde{\sigma}\rangle \langle FS, \sigma|) \quad (44)$$

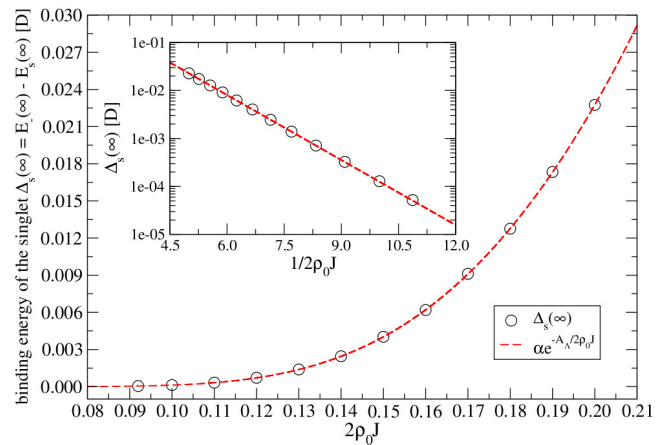


FIG. 10. (Color online) Binding energy of the singlet state $\Delta_s(\infty) = E_-(\infty) - E_s(\infty)$ with E_- and E_s from Eqs. (45a) and (28) for the Kondo model with $N = 40$ and $\Lambda = 2$. The binding energy shows the generic exponential behavior $\Delta_s(\infty) \propto \exp(A_\Lambda/2\rho_0J)$. The factor A_Λ from (22) is an effect of the discretization.

where we have first diagonalized the non-diagonal terms proportional to E_{kq} . Diagonalizing the terms $|k\rangle \langle q|$ yields the eigenvalues

$$E_{s\pm}, \quad E_{t_{1,2,3}\pm} \\ E_{\pm} = \frac{1}{2} \left[E_{\text{FS},\sigma} + E_{\tilde{\sigma}} \pm \sqrt{(E_{\text{FS},\sigma} - E_{\tilde{\sigma}})^2 + 4g^2} \right] \quad (45a)$$

where the lowest-lying level is the energy of the singlet E_s and the second lowest-lying is the energy level E_- which belongs to a linear combination of the Fermi sea and the $|\tilde{\sigma}\rangle$ -states, see also (28).

Fig. 9 depicts the corresponding flow of $\Delta_s(l)$. The energy necessary to break up the singlet ground state is given by the difference

$$\Delta_s(\infty) = E_-(\infty) - E_s(\infty) \quad (46)$$

where E_s is the singlet energy, which is the lowest lying state, and E_- is given by (45a), which is the first excitation above the singlet state *involving* the impurity. We draw the reader's attention to the fact that Δ_s can only be interpreted as the binding energy for $l \rightarrow \infty$ because only then the ground state of the effective model will be the singlet state. For smaller l there are still interaction terms present that act on the singlet state which vanish in the limit $l \rightarrow \infty$.

Upon increasing l , $\Delta_s(l)$ increases rapidly until it converges towards the binding energy of the singlet state $\Delta_s(\infty)$. The binding energy is analyzed in Fig. 10. For $l \rightarrow \infty$ we find an exponential behavior of the form

$$\Delta_s(\infty) \propto e^{-\frac{A_\Lambda}{2\rho_0 J}} \quad (47)$$

where the discretization factor A_Λ is given by (22).

Hence, we conclude that the modified CUT approach not only yields an effective Hamiltonian with finite couplings, but also results in a model in which the Kondo energy scale is already manifest in the diagonal part. It is no longer hidden within the intricate interplay of different physical processes.

Recall that earlier CUT approaches led to diverging couplings²³ or to an effective model where the parameters exhibited logarithmic infrared divergences very similar to those found by a standard perturbative treatment¹. Alternatively, the detour via a bosonized form of the Kondo model was taken^{25–27}. The mapping of the fermionic Kondo model to the bosonized one is systematically controlled only in the wide band limit.

IV. ANDERSON IMPURITY MODEL

In the last two sections we considered the Kondo model first in the standard CUT akin to poor man's scaling and second with a change of reference state. The first approach yields diverging couplings while the second provides a well-defined effective model with finite couplings. In the present section and in the next one we will extend these treatments to the Anderson impurity model.

A. Parametrization of the Anderson impurity model

We consider the Anderson impurity model in its standard form^{2,3}

$$H = \sum_{\mathbf{k},\sigma} \epsilon_{\mathbf{k}} c_{\mathbf{k}\sigma}^\dagger c_{\mathbf{k}\sigma} + \sum_{\sigma} \epsilon_d d_{\sigma}^\dagger d_{\sigma} + U d_{\uparrow}^\dagger d_{\downarrow}^\dagger d_{\downarrow} d_{\uparrow} + \sum_{\mathbf{k},\sigma} \left(V_{\mathbf{k}} d_{\sigma}^\dagger c_{\mathbf{k}\sigma} + V_{\mathbf{k}}^* c_{\mathbf{k}\sigma}^\dagger d_{\sigma} \right). \quad (48)$$

If we discretize it in the energy representation employing the formulae (8a) we obtain

$$H = \sum_{s=\pm} \sum_{n,\sigma} \epsilon_n^s c_{n\sigma}^\dagger c_{n\sigma,s} + \epsilon_d \sum_{\sigma} d_{\sigma}^\dagger d_{\sigma} + U d_{\uparrow}^\dagger d_{\downarrow}^\dagger d_{\downarrow} d_{\uparrow} + \sum_{s=\pm} \sum_{n,\sigma} V \gamma_n^s (c_{n\sigma,s}^\dagger d_{\sigma} + d_{\sigma}^\dagger c_{n\sigma,s}). \quad (49)$$

The Schrieffer-Wolff transformation to a Kondo-type model has been realized already in the early days of CUTs³⁰ and extended recently to superconducting hosts³². Here, we use a slightly different approach to eliminate the hybridization elements V_n . We consider a discretized flat density of states (DOS) (49) and choose the ground state of

$$H_D = \sum_{n,\sigma} \epsilon_n c_{n\sigma}^\dagger c_{n\sigma} + \epsilon_d \sum_{\sigma} n_{d,\sigma} + U n_{d,\uparrow} n_{d,\downarrow} \quad (50)$$

as the reference state where $n_{d,\sigma}$ is the occupation operator of the d -level

$$n_{d,\sigma} = d_{\sigma}^\dagger d_{\sigma}. \quad (51)$$

In the present article, we restrict ourselves to the particle-hole symmetric cases. Then, the singly occupied impurity state is the lowest-lying eigenstate of (50) and thus there are two degenerate reference states with a spin degree of freedom at the impurity. Hence we have to use a reference ensemble for the impurity operators and the normal-ordering scheme employed is defined by

$$\langle \uparrow | : \hat{A} : | \uparrow \rangle + \langle \downarrow | : \hat{A} : | \downarrow \rangle = 0. \quad (52)$$

In order to be able to use sign generators similar to (16), it must be evident which change of energy they induce. The sign of this energy change determines the sign of the term in the generator. To this end, we introduce an operator basis whose terms imply a unambiguous change of local energy on the impurity. The chosen operator basis has already been used successfully before in the derivation of generalized t - J models from Hubbard models⁴⁰. Its terms are shown in Tab. I.

bosonic operators	fermionic operators
$\mathbb{1}$	$F_{1,\uparrow} = (1 - n_{d,\downarrow}) d_{\uparrow}$
$n_z = n_{d,\uparrow} - n_{d,\downarrow}$	$F_{1,\downarrow} = (1 - n_{d,\uparrow}) d_{\downarrow}$
$d_{\uparrow}^\dagger d_{\downarrow}$	$F_{2,\uparrow} = n_{d,\downarrow} d_{\uparrow}$
$d_{\downarrow}^\dagger d_{\uparrow}$	$F_{2,\downarrow} = n_{d,\uparrow} d_{\downarrow}$
$d_{\downarrow} d_{\uparrow}$	$F_{2,\uparrow}^\dagger = n_{d,\downarrow} d_{\uparrow}^\dagger$
$d_{\uparrow}^\dagger d_{\downarrow}^\dagger$	$F_{2,\downarrow}^\dagger = n_{d,\uparrow} d_{\downarrow}^\dagger$
$\bar{n} = n_{d,\uparrow} + n_{d,\downarrow} - \mathbb{1}$	$F_{1,\uparrow}^\dagger = (1 - n_{d,\downarrow}) d_{\uparrow}^\dagger$
$\hat{D} = 2n_{d,\uparrow} n_{d,\downarrow} - \bar{n}$	$F_{1,\downarrow}^\dagger = (1 - n_{d,\uparrow}) d_{\downarrow}^\dagger$

TABLE I. Impurity operator basis with $n_{d,\sigma} = d_{\sigma}^\dagger d_{\sigma}$.

The reason for this choice of operator basis becomes evident upon inspecting the local impurity configurations which are connected by these operators. The energy difference between the empty and the singly occupied state is different from the energy difference between the singly and the doubly occupied state. Thus, there is no unique energy change induced by the operator d_{σ}^\dagger because it connects the empty to the singly occupied state and the singly occupied to the doubly occupied state.

The projected operator $F_{1,\sigma}^\dagger = (1 - n_{\bar{\sigma}}) d_{\sigma}^\dagger$ only connects the empty to the singly occupied state while the projected operator $F_{2,\sigma}^\dagger = n_{\bar{\sigma}} d_{\sigma}^\dagger$ only connects the singly occupied to the doubly occupied state. Thus, there are unambiguous energy differences induced by the projected operators reading

$$\Delta E_1 = \epsilon_d = \tilde{\epsilon}_d - \tilde{U} \quad (53a)$$

$$\Delta E_2 = \epsilon_d + U = \tilde{\epsilon}_d + \tilde{U} \quad (53b)$$

where the coefficients \tilde{U} and $\tilde{\epsilon}_d$ are the coefficients of the Anderson impurity Hamiltonian (54) expressed in the operator basis given in Tab. I. The values of the coefficients are given in (56).

The Anderson impurity Hamiltonian expressed in the projected impurity operator basis takes the form

$$H = H_D + H_R \quad (54)$$

with the diagonal part H_D and the hybridization part H_R

$$H_D = \sum_{n,\sigma} \epsilon_n : c_{n\sigma}^\dagger c_{n\sigma} : + \tilde{\epsilon}_d \bar{n} + \tilde{U} \hat{D} \quad (55a)$$

$$H_R = \sum_{n,\sigma} V_n \left(F_{1\sigma}^\dagger c_{n\sigma} + c_{n\sigma}^\dagger F_{1\sigma} \right) + \sum_{n,\sigma} \Gamma_n \left(F_{2\sigma}^\dagger c_{n\sigma} + c_{n\sigma}^\dagger F_{2\sigma} \right). \quad (55b)$$

The coefficients in the projected operator basis are given by

$$V_n = V\gamma_n, \quad \Gamma_n = V\gamma_n, \quad \tilde{\epsilon}_d = \epsilon_d + \frac{U}{2}, \quad \tilde{U} = \frac{U}{2} \quad (56)$$

with the parameters ϵ_n and γ_n from (14a). The fermionic bath operators are still normal-ordered with respect to the Fermi sea.

B. Elimination of the hybridization

We want to eliminate the hybridization elements and analyze the spin-spin interaction induced thereby. This amounts up to the Schrieffer-Wolff transformation realized by CUTs³⁰ or the systematic derivation of t - J models from Hubbard models by CUTs⁴⁰. We choose the generator

$$\eta = \sum_{n,\sigma} \eta_n^V \left(F_{1\sigma}^\dagger c_{n\sigma} - c_{n\sigma}^\dagger F_{1\sigma} \right) + \sum_{n,\sigma} \eta_n^\Gamma \left(F_{2\sigma}^\dagger c_{n\sigma} - c_{n\sigma}^\dagger F_{2\sigma} \right) + \sum_{n,m,\sigma} \eta_{nm}^t : c_{n\sigma}^\dagger c_{m\sigma} :. \quad (57)$$

For the flow equation (2) we commute the generator (57) with the Hamiltonian (54) which generates terms not present in the initial Hamiltonian reading

$$H_t = \sum_{n,m,\sigma} t_{nm} : c_{n\sigma}^\dagger c_{m\sigma} : \quad (58a)$$

$$H_J = \sum_{n,m,\sigma} J_{nm}^{\uparrow\downarrow} d_\sigma^\dagger d_\sigma c_{n\bar{\sigma}}^\dagger c_{m\sigma} + \sum_{n,m,\sigma} J_{nm}^{n_z} n_z : c_{n\sigma}^\dagger c_{m\sigma} : + \sum_{n,m,\sigma} J_{nm}^{\bar{n}} \bar{n} : c_{n\sigma}^\dagger c_{m\sigma} : + \sum_{n,m} J_{nm}^\pm \left(d_\uparrow^\dagger d_\downarrow^\dagger c_{n\downarrow} c_{m\uparrow} + c_{m\uparrow}^\dagger c_{n\downarrow}^\dagger d_\downarrow d_\uparrow \right). \quad (58b)$$

All these emerging terms are of order V^2 and coincide with terms in the arising in the standard Schrieffer-Wolff transformation⁴⁸. We aim at computing the couplings $J_{nm}^{(i)}$ from (58a) in order V^2 and thus the commutators

$$[\eta_R, H_D + H_R] \quad \text{and} \quad [\eta_t, H_D] \quad (59)$$

are needed; all other commutations yield terms of order V^3 or higher.

Aiming at H_J from (58a) in order V^2 we neglect all terms which contribute to H_J in order V^3 . We point out that this implies also to neglect terms in order V^2 which are not of the form H_J and will influence H_J only in order V^3 or higher. This argument applies to the flow of H_D and the emerging hopping terms t_{nm} because they lead to corrections to H_J of order V^3 and higher only. In this way, the flow equations simplify to

$$\partial_t V_n = \eta_n^V \left(\epsilon_n - \tilde{\epsilon}_d + \tilde{U} \right) \quad (60a)$$

$$\partial_t \Gamma_n = \eta_n^\Gamma \left(\epsilon_n - \tilde{\epsilon}_d - \tilde{U} \right) \quad (60b)$$

$$\partial_t J_{nm}^{\uparrow\downarrow} = \eta_n^\Gamma \Gamma_m + \eta_m^\Gamma \Gamma_n - \eta_n^V V_m - \eta_m^V V_n \quad (60c)$$

$$\partial_t J_{nm}^\pm = \eta_n^\Gamma V_m + \eta_m^\Gamma V_n - \eta_n^V \Gamma_m - \eta_m^V \Gamma_n \quad (60d)$$

where only $J_{nm}^{\uparrow\downarrow}$ has to be known due to spin-rotation symmetry

$$\sigma J_{nm\sigma}^{n_z} = \frac{1}{2} J_{nm}^{\uparrow\downarrow}. \quad (61)$$

The operator $F_{1\sigma}^\dagger c_{n\sigma}$ promotes the empty impurity state to the singly occupied one while annihilating a particle with energy ϵ_n in the bath. This leads to a change of energy

$$\Delta E_{1,n} = \tilde{\epsilon}_d - \tilde{U} - \epsilon_n. \quad (62)$$

The operator $F_{2\sigma}^\dagger c_{n\sigma}$ promotes the singly occupied to the doubly occupied impurity level and annihilates a particle with energy ϵ_n in the bath. This implies a change of energy

$$\Delta E_{2,n} = \tilde{\epsilon}_d + \tilde{U} - \epsilon_n. \quad (63)$$

Thus, the sign generator takes the form

$$\eta_n^V = -\text{sgn} \left(\epsilon_n - \tilde{\epsilon}_d + \tilde{U} \right) V_n \quad (64a)$$

$$\eta_n^\Gamma = -\text{sgn} \left(\epsilon_n - \tilde{\epsilon}_d - \tilde{U} \right) \Gamma_n. \quad (64b)$$

C. Diagonalization of the induced spin-spin interaction

In addition, we want to diagonalize the induced spin-spin interaction at the same time as it is generated upon eliminating the hybridization. For this reason, we add the following terms to the generator

$$\eta_J = \sum_{n,m,\sigma} \eta_{nm}^{\uparrow\downarrow} d_\sigma^\dagger d_\sigma c_{n\bar{\sigma}}^\dagger c_{m\sigma} + \sum_{n,m,\sigma} \eta_{nm}^{n_z} n_z : c_{n\sigma}^\dagger c_{m\sigma} : + \sum_{n,m} \eta_{nm}^\pm \left(d_\uparrow^\dagger d_\downarrow^\dagger c_{n\downarrow} c_{m\uparrow} - c_{m\uparrow}^\dagger c_{n\downarrow}^\dagger d_\downarrow d_\uparrow \right) + \sum_{n,m,\sigma} \eta_{nm}^{\bar{n}} \bar{n} : c_{n\sigma}^\dagger c_{m\sigma} :. \quad (65)$$

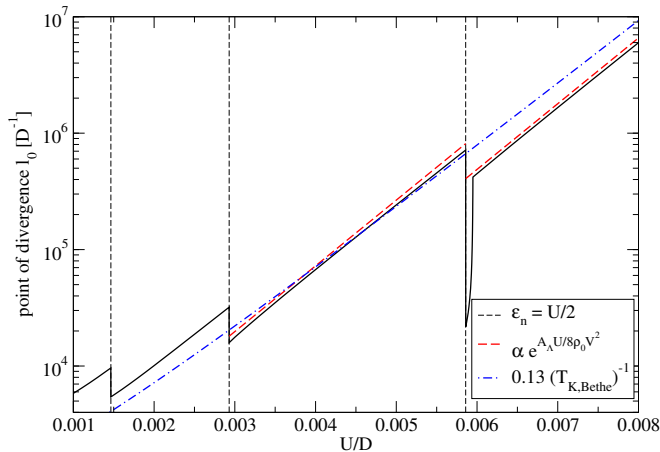


FIG. 11. (Color online) Flow parameter l_0 at which the flow equation diverges (compare Fig. 2) for the Anderson impurity model with $N = 60$, $\Lambda = 2$ and $V/D = 0.01414$ in a logarithmic plot vs. U/D . The inverse energy l_0 shows the generic exponential behavior $l_0 \propto \exp(A_\Lambda U/8\rho_0 V^2)$ of the Kondo temperature T_K of the Anderson impurity model. The factor A_Λ is given by (22). The dashed-dotted curve (blue) depicts the Bethe ansatz result (71).

The discontinuous behavior is a result of the discretization and happens every time when $U/2$ crosses an energy level ϵ_n (dotted vertical lines). For decreasing Λ the discontinuities become smaller (compare Fig. 12).

These terms lead in the sign generator to terms of the same kind with the prefactors

$$\eta_{mm}^{\uparrow\downarrow} = \text{sgn}(\epsilon_n - \epsilon_m) J_{nm}^{\uparrow\downarrow} \quad (66a)$$

$$\eta_{nm}^{nz} = \text{sgn}(\epsilon_n - \epsilon_m) J_{nm}^{nz} \quad (66b)$$

$$\eta_{nm\sigma}^{\bar{n}} = \text{sgn}(\epsilon_n - \epsilon_m) J_{nm}^{\bar{n}} \quad (66c)$$

$$\eta_{mm}^{\pm} = -\text{sgn}(\epsilon_n + \epsilon_m) J_{nm}^{\pm} \quad (66d)$$

We only track terms that act in lowest order J^2 on the spin-spin interaction neglecting higher order contributions in J . Hence the commutators $[\eta_J, H_D + H_J]$ are needed. Among the resulting terms only the terms are kept that act on H_J . All other terms are neglected because their feedback on the spin-spin interaction is at least of order J^3 . Calculating the commutators and comparing the coefficients in the flow equation (2) yields additional terms to the flow equation (60) so that one arrives

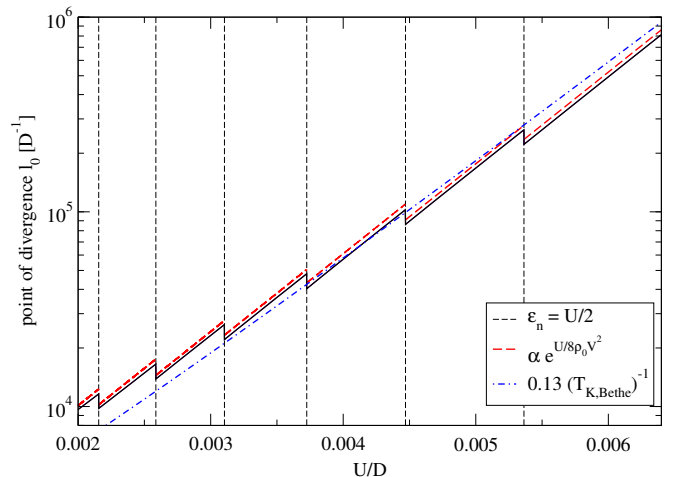


FIG. 12. (Color online) Flow parameter l_0 at which the flow equation diverges (cf. Fig. 2) for the Anderson impurity model with $N = 200$, $\Lambda = 1.2$ and $V/D = 0.01414$ in a logarithmic plot vs. U/D . The inverse energy l_0 displays the generic exponential character $l_0 \propto \exp(A_\Lambda U/8\rho_0 V^2)$ of the Kondo temperature T_K of the Anderson impurity model. The discretization factor A_Λ is given by (22). The dashed-dotted curve (blue) depicts the Bethe ansatz result (71). The discontinuous behavior is a result of the discretization and occurs each time when $U/2$ crosses an energy level ϵ_n (dotted vertical lines).

at

$$\begin{aligned} \partial_l J_{nm\sigma}^{nz} &= (\epsilon_m - \epsilon_n) \eta_{nm\sigma}^{nz} \\ &\quad - \frac{1}{2} \sum_x \sigma (\eta_{nx}^{\uparrow\downarrow} J_{xm}^{\uparrow\downarrow} - \eta_{xm}^{\uparrow\downarrow} J_{nx}^{\uparrow\downarrow}) (1 - 2\theta_x) \end{aligned} \quad (67a)$$

$$\begin{aligned} \partial_l J_{nm}^{\uparrow\downarrow} &= (\epsilon_m - \epsilon_n) \eta_{nm}^{\uparrow\downarrow} \\ &\quad + \sum_x \sigma (\eta_{xm\sigma}^{nz} J_{nx}^{\uparrow\downarrow} - \eta_{nx\sigma}^{nz} J_{xm}^{\uparrow\downarrow}) (1 - 2\theta_x) \\ &\quad + \sum_x \sigma (\eta_{xm}^{\uparrow\downarrow} J_{nx\sigma}^{nz} - \eta_{nx}^{\uparrow\downarrow} J_{xm\sigma}^{nz}) (1 - 2\theta_x) \end{aligned} \quad (67b)$$

$$\begin{aligned} \partial_l J_{nm}^{\bar{n}} &= (\epsilon_m - \epsilon_n) \eta_{nm}^{\bar{n}} \\ &\quad - \frac{1}{2} \sum_x (\eta_{xn}^{\pm} J_{xm}^{\pm} + \eta_{xm}^{\pm} J_{xn}^{\pm}) (1 - 2\theta_x) \end{aligned} \quad (67c)$$

$$\begin{aligned} \partial_l J_{nm}^{\pm} &= (\epsilon_n + \epsilon_m) \eta_{nm}^{\pm} \\ &\quad + \sum_x (\eta_{xm\uparrow}^{\bar{n}} J_{nx}^{\pm} + \eta_{xn\downarrow}^{\bar{n}} J_{xm}^{\pm}) (1 - 2\theta_x) \\ &\quad - \sum_x (\eta_{nx}^{\pm} J_{xm\uparrow}^{\bar{n}} + \eta_{xm}^{\pm} J_{xn\downarrow}^{\bar{n}}) (1 - 2\theta_x) \end{aligned} \quad (67d)$$

where σ labels the spin if it is used as index while it takes the values $\sigma = \pm 1$ as a coefficient. The occupation number

$$\theta_x = \langle c_{x\sigma}^\dagger c_{x\sigma} \rangle \quad (68)$$

is calculated with respect to the Fermi sea and results from the normal-ordering of the fermionic bath operators.

Taking a closer look at the flow equation (67) reveals that J^{nz} and $J^{\uparrow\downarrow}$ only influence each other. They do not

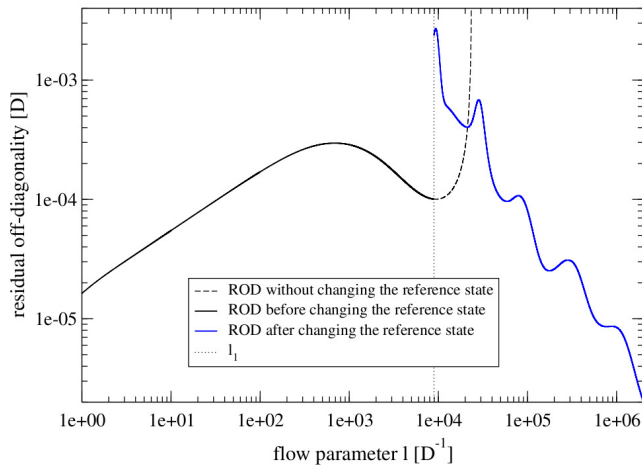


FIG. 13. (Color online) ROD for the Anderson impurity model with $N = 52$, $\Lambda = 2$, $U/D = 3.2 \cdot 10^{-3}$, and $V/D = 0.01414$. The first part of the flow only shows the ROD of (70) for the induced spin-spin interaction $J_{nm}^{\uparrow\downarrow}$ from (58a). The diagonalization of the induced spin-spin interaction leads to the divergence depicted as dashed black line. After changing the reference state we solve the flow (39) which turns out to converge in contrast to the original flow (70).

couple to J^{\pm} or $J^{\bar{n}}$ which also only influence each other. The spin-rotation symmetry

$$\sigma J_{nm\sigma}^{nz} = \frac{1}{2} J_{nm}^{\uparrow\downarrow} \quad (69)$$

holds true during the whole flow which simplifies the flow equation for $J_{nm}^{\uparrow\downarrow}$ to

$$\partial_l J_{nm}^{\uparrow\downarrow} = -(\epsilon_n - \epsilon_m) \eta_{nm}^{\uparrow\downarrow} - \sum_x (\eta_{nx}^{\uparrow\downarrow} J_{xm}^{\uparrow\downarrow} - \eta_{xm}^{\uparrow\downarrow} J_{nx}^{\uparrow\downarrow}) (1 - 2\theta_x). \quad (70)$$

This differential equation is the same as Eq. (17) which is the flow equation for the diagonalization of the spin-spin interactions in the Kondo model. Recall that in the Anderson impurity model we aim at eliminating the charge fluctuations induced by the hybridization V_{nm} and diagonalizing the induced spin-spin interaction J_{nm} simultaneously. We emphasize that this is not in one-to-one correspondence to applying a Schrieffer-Wolff transformation first and then diagonalizing the effective Kondo Hamiltonian.

In order to determine the Kondo energy scale of the Anderson impurity Hamiltonian with CUTs we combine (60), and (67). This flow equation also leads to divergence on an energy scale that depends on the parameters U and V . Fig. 11 shows the point of divergence l_0 as function of the interaction U . There are certain values of U for which discontinuous jumps occur. In the intervals between the discontinuities we find the correct exponential behavior of the Kondo temperature $T_k^{-1} \propto \exp(A_{\Lambda} \frac{U}{8\rho_0 V^2})$ where A_{Λ} from (22) captures the influence of the discretization on the Kondo temperature, cf. Ref. 9. In order to show that the overall behavior is indeed the correct

one, Fig. 11 also depicts the Bethe ansatz result^{3,11}

$$T_{K,\text{Bethe}} = U \sqrt{\frac{\Delta}{2A_{\Lambda}U}} \exp\left(-\frac{\pi A_{\Lambda}U}{8\Delta} + \frac{\pi\Delta}{2A_{\Lambda}U}\right) \quad (71)$$

where we use the hybridization $\Delta = \pi V^2/(2D)$ as usual shorthand. Moreover we introduced the discretization factor A_{Λ} wherever the ratio U/Δ occurs.

The origin of the discontinuities is the discretization of the bare energy levels. Each time the interaction $\frac{U}{2}$ crosses an energy level ϵ_n , one sign in the generator

$$\eta_n^V = -\text{sgn}(\epsilon_n + U/2) V_n \quad (72a)$$

$$\eta_n^{\Gamma} = -\text{sgn}(\epsilon_n - U/2) \Gamma_n \quad (72b)$$

is changed discontinuously implying a discontinuity in all other quantities as well.

In Figs. 11 and 12 the dashed vertical lines show the values of the interaction where $\frac{U}{2} = \epsilon_n$. One clearly sees that the discontinuities occur indeed exactly when $\frac{U}{2}$ crosses an energy level ϵ_n . In Fig. 12 the discretization parameter Λ is decreased and thus more energy levels lie in the considered interval. As a result more discontinuities occur, but the weight $|\gamma_n|^2$ carried by the respective energy levels decreases so that the induced jumps become smaller. Thus, in the limit of $\Lambda \rightarrow 1$ the curve would not display jumps anymore.

Summarizing this section, we succeeded in eliminating the hybridization in the Anderson impurity model by means of a continuous unitary transformation and the thus induced spin-spin interaction until a small energy scale (large values of the flow parameter l) where the flow diverges. This energy scale turns out to be the Kondo energy scale T_K , capturing the correct exponential behavior in U

$$T_K = l_0^{-1} = C(U) \exp\left(-A_{\Lambda} \frac{U}{8\rho_0 V^2}\right) \quad (73)$$

where $C(U)$ stems from the discretization and describes the discontinuous behavior observed in Figs. 11 and 12; $C(U)$ is constant in each interval between two discontinuities. The factor A_{Λ} captures the discretization corrections in the exponent⁹. To our knowledge, the correct exponential scale has not yet been found by a CUT so far. Still, we do not obtain a finite effective model, but a divergent flow.

V. MODIFIED APPROACH TO THE ANDERSON IMPURITY MODEL

Here, we apply the modified approach to the Anderson impurity model. First we follow the procedure of the last section and start from the Anderson impurity Hamiltonian in the form (54). The hybridization is eliminated by using (60). Simultaneously, the thus induced spin-spin interaction is diagonalized by using (70). For small values of the flow parameter l the spin-spin exchange couplings $J_{nm}^{\uparrow\downarrow}$ are generated in the process of the elimination of the hybridization elements.

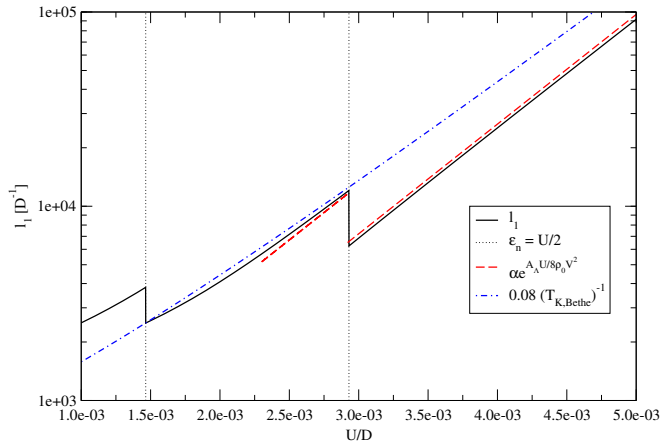


FIG. 14. (Color online) Inverse energy scale l_1 at which the reference state is changed for the Anderson impurity model with $N = 52$, $\Lambda = 2$ and $V/D = 0.01414$. The inverse energy scale l_1 is increasing proportional to the inverse of the Kondo temperature $T_K^{-1} \propto \exp(A_\Lambda U/8\rho_0 V^2)$. The dashed-dotted curve (blue) depicts the Bethe ansatz result (71). The factor A_Λ from (22) takes the discretization into account. The discontinuities stem also from the discretization of the energy.

Beyond some value of l the hybridization elements become negligible. Then the backaction of the induced spin-spin interaction on itself in (70) is the driving effect in the flow equation which leads to diverging couplings (dashed black line in Fig. 13). At an even larger value l_1 the formation of a singlet state with the impurity becomes energetically favorable. This is determined just as in the case of the Kondo model referring to the coupling $J_{nm}^{\uparrow\downarrow}$ instead of J_{nm} . To this end, we consider only the singly occupied impurity state because l_1 is much larger than $1/U$ so that the charge fluctuations on the impurity will not play any significant role at this stage of the flow. Hence the couplings J_{nm}^\pm and $J_{nm}^{\bar{n}}$ do not need to be considered beyond l_1 . Using the spin-rotation symmetry (69) for $J_{nm}^{n_z}$ and $J_{nm}^{\uparrow\downarrow}$ leads to an effective Kondo Hamiltonian with the couplings $J_{nm} = J_{nm}^{\uparrow\downarrow}$. Subsequently, we can follow the same procedure as in the Kondo model, i.e., we change the reference state to a mixture of singlets between the impurity spin and bath fermions at the Fermi level and we expand the effective Kondo Hamiltonian in the modified operator basis (27) and use the modified flow equation (39).

Fig. 13 shows the ROD of the Anderson impurity model obtained with this modified approach. We only plot the ROD of the spin-spin couplings

$$\text{ROD}^2 = \sum_{\substack{n,m \\ n \neq m}} |J_{nm}^{\uparrow\downarrow}|^2. \quad (74)$$

First, the ROD is increasing because the spin-spin coupling is generated by the elimination of the hybridization. Without changing the reference state the flow equation (70) leads to divergence, see dashed black line. At some point l_1 before the divergence occurs the singlet forma-

tion becomes energetically favorable, see Eq. (30), and the reference state is changed.

The ROD shows a discontinuous behavior when the reference state is changed because we use the modified generator which includes additional terms. The reason why the ROD is abruptly increasing is the same as in the case of the Kondo model, see Sect. III B. In contrast to the flow without change of reference state, the modified flow equation converges and leads to a finite, well-defined effective Hamiltonian. Next, we analyze the same energy scales as for the Kondo model.

A. Effective model for the Anderson impurity model

Fig. 14 shows the flow parameter l_1 at which the reference state is changed. We again find discontinuities for the same reason as they occurred in Fig. 11. Between two discontinuities we find the exponential behavior characteristic of the Kondo energy scale in the Anderson impurity model

$$l_1^{-1} \propto \exp\left(-A_\Lambda \frac{U}{8\rho_0 V^2}\right). \quad (75)$$

Thus, for the Anderson impurity model the point where the reference state is changed is also given by the Kondo temperature T_K .

B. Binding energy of the Kondo singlet

In Fig. 15 the flow of Δ_s from (42) is displayed. Discontinuities occur whenever $U/2$ an energy level ϵ_n . For clarity the different regions between two consecutive values of ϵ_n are depicted in two panels in Fig. 15. We find that Δ_s increases quickly and converges to the binding energy of the singlet $\Delta_s(\infty)$.

The binding energy of the singlets is analyzed in Fig. 16. We again find the discontinuities already observed in Fig. 11. Between these discontinuities the binding energy decreases according to

$$\Delta_s(\infty) \propto \exp\left(-A_\Lambda \frac{U}{8\rho_0 V^2}\right). \quad (76)$$

Thus, we again retrieve a singlet ground state with a binding energy given by the Kondo temperature T_K .

VI. SUMMARY

A. Conclusions

To treat the exponentially small Kondo energy scale reliably is a key problem in correlated fermionic systems. We presented a way how to use CUTs in order to derive effective models for the Kondo and the Anderson

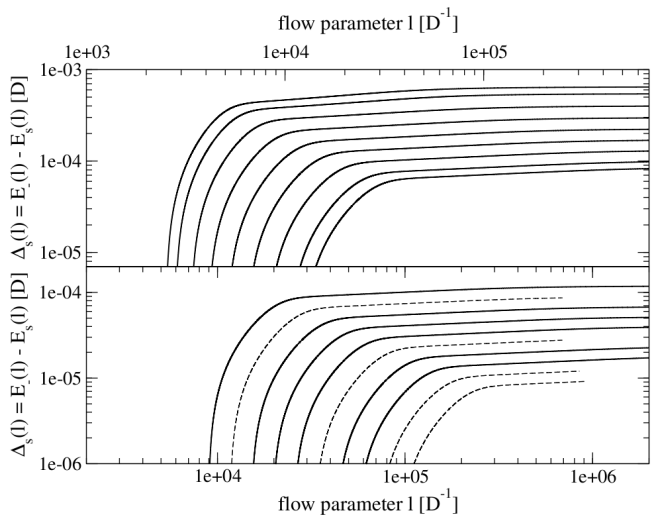


FIG. 15. (Color online) Flow of $\Delta_s(l) = E_-(l) - E_s(l)$ where E_- and E_s result from (45a) and (28) for the Anderson impurity model with $N = 52$, $\Lambda = 2$ and $V/D = 0.01414$ and various values of the interaction. From top to bottom: (upper panel) $U/D \cdot 10^3 = 1.464, 1.6, 1.8, 2, 2.2, 2.4, 2.6, 2.8, 2.929$, (lower panel) $U/D \cdot 10^3 = 3.2, 3.4, 3.6, 3.8, 4, 4.2, 4.4, 4.6, 4.8, 5$. The energy difference Δ_s converges to the binding energy of the Kondo singlet for $l \rightarrow \infty$. The flow for the different parameters is split into two plots for clarity because each time when $U/2$ crosses ϵ_n l_0 jumps, cf. Fig. 16.

impurity model. The conventional CUT approach with a fixed reference state leads to diverging flow equations²³. We identified the origin of this divergence which lies in the inappropriate reference state. We introduced a modified approach based on the change of the reference state for the Kondo and the Anderson impurity model which solves the problem of diverging couplings during the flow and results in a well-behaved effective low-energy model with finite parameters at arbitrarily small energies. This is the main achievement of the present work. We find a singlet ground state with a binding energy that is given by the Kondo temperature T_K . Our approach is able to capture the exponentially small Kondo energy scale. The quantitative result for the Anderson impurity model compares well with the Bethe ansatz result^{3,11}.

The ground state of the effective model obtained by the CUT is a singlet and a Fermi sea. But we stress that the complete effective model also comprises couplings between the triplet states of the impurity and the fermions in the bath. This implies that even the effective model represents a correlated problem with non-trivial properties. Furthermore, interactions within the fermionic bath have not been tracked. For these reasons it is beyond the scope of the present work to analyze other characteristic quantities such as the Wilson ratio and the like.

Earlier approaches for the Kondo model result in diverging couplings at a characteristic flow parameter²³, an effective model where the parameters still exhibit loga-

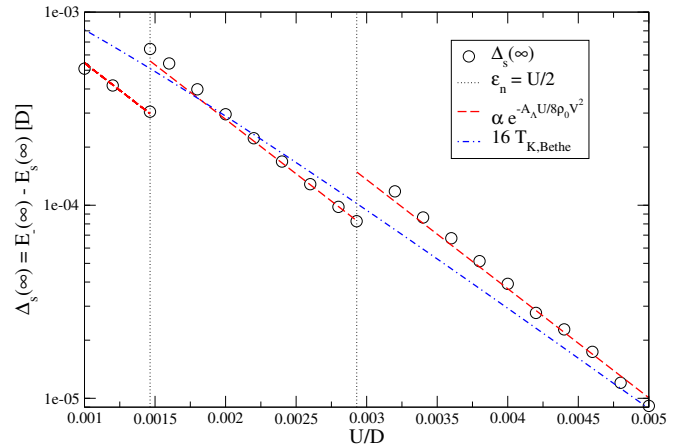


FIG. 16. (Color online) Binding energy of the singlet $\Delta_s(\infty) = E_-(\infty) - E_s(\infty)$ with E_- and E_s from (45a) and (28) for the Anderson impurity model with $N = 52$, $\Lambda = 2$ and $V/D = 0.01414$. The binding energy shows the exponential behavior $\Delta_s(\infty) \propto \exp(-A_\Lambda U / 8\rho_0 V^2)$. The dashed-dotted curve (blue) depicts the Bethe ansatz result (71). The factor A_Λ from (22) takes the effects of discretization into account.

arithmic infrared divergences²⁴ or rely on a bosonized form of the Kondo model before applying the CUT²⁵⁻²⁷.

In the case of the Anderson impurity model, only a few approaches based on CUTs were published^{28,30,31} while none of them reveal the exponential character of the Kondo temperature T_K . Nevertheless, an important previous work is able to reconstruct the Schrieffer-Wolff transformation using CUTs³⁰ and can be extended to other hosts³². Our approach does not rely on a bosonized form and can be extended to the Anderson impurity model.

Of course, there are other methods which reliably provide the exponentially small Kondo energy. The first is the numerical renormalization group⁸⁻¹⁰ and the Bethe ansatz solution¹¹. But the challenge to find a reliable RG approach with convergent flow has continued to attract much attention. The functional RG approach yielded good results up to intermediate interactions for the Anderson impurity model¹². Many other studies¹³⁻¹⁷ improved the functional RG approach recently but did not capture the strong coupling regime. Only in 2013, Streib and co-workers succeeded¹⁸ exploiting a magnetic field as regulatory cutoff and conserved Ward identities similar to a renormalized perturbation theory developed by Hewson and his co-workers¹⁹⁻²¹. The difficulties that these intricate approaches had to face underlines impressively that the Kondo effect in the Anderson impurity problem represents a true challenge.

The modified approach based on CUTs advocated here has the merit to provide a convergent, i.e., with finite coefficients, effective low-energy models of the Anderson impurity model and the Kondo model. The key element is the change of the reference state capturing the exponential character of the Kondo temperature. This is the

central finding of our study.

B. Outlook

Several extensions suggest themselves. One route is to extend the set of operators to capture more than the leading processes in the two main parts of the transformation: (i) the elimination of the hybridization governed by the expansion in V and (ii) the renormalization of the exchange couplings J by eliminating the non-diagonal exchange couplings²³. By such an extension, higher order corrections beyond V^2 and J^2 can be addressed and the results for the Kondo energy scale can be improved quantitatively.

A second route is to further explore the properties of the obtained effective model. For instance, it is interesting to compute explicitly the impurity contribution to the magnetic susceptibility χ and to the specific heat C . We stress, however, that the analysis of the effective model is not straightforward because it still represents a correlated problem, for instance, due to the interactions between the triplet states of the impurity and the fermions in the bath. If χ and C are known quantitatively the characteristic Wilson ratio is known which is an established measure for the degree of correlation effects. The technical difficulty in the CUTs is to separate

the contribution of the impurity in the renormalization of the effective parameters.

A third route is to tackle the transformation of the observables as well. Transforming the creation and annihilation operator of the impurity fermion will allow us to compute the spectral densities which is a decisive quantity in many applications³⁻⁷.

A fourth extension is to address the case of the asymmetric Anderson impurity model where the particle-hole asymmetry is broken³ and fifth extension is to address finite temperatures as well.

Finally, we think that the methodological progress developed for the treatment of the Kondo problem by continuous unitary transformations will trigger improved approaches to other strongly correlated problems in general. Examples are extended correlated systems with massless excitations or the vicinities of quantum phase transitions where the ground state has to be switched just as the reference state has to be switched in the present study.

ACKNOWLEDGMENTS

We thank Frithjof B. Anders, Nils A. Drescher and Sebastian Schmitt for many useful discussions. Financial support by the Helmholtz Virtual Institute “New states of matter and their excitations” is acknowledged.

* joern.krones@tu-dortmund.de

† goetz.uhrig@tu-dortmund.de

¹ J. Kondo, Prog. Theor. Phys. **32**, 37 (1964).

² P. W. Anderson, Phys. Rev. **124**, 41 (1961).

³ A. C. Hewson, *The Kondo Problem to Heavy Fermions* (Cambridge University Press, Cambridge, 1993).

⁴ G. R. Stewart, Rev. Mod. Phys. **56**, 755 (1984).

⁵ M. J. Rozenberg, X. Y. Zhang, and G. Kotliar, Phys. Rev. Lett. **69**, 1236 (1992).

⁶ A. Georges, G. Kotliar, W. Krauth, and M. J. Rozenberg, Rev. Mod. Phys. **68**, 13 (1996).

⁷ M. Grobis, I. G. Rau, R. M. Potok, and D. Goldhaber-Gordon, *Kondo Effect in Mesoscopic Quantum Dots*, edited by H. Kronmüller and S. Parkin, Handbook of Magnetism and Advanced Magnetic Materials, Vol. 5 (Wiley, 2007).

⁸ K. G. Wilson, Rev. Mod. Phys. **47**, 773 (1975).

⁹ H. R. Krishna-murthy, J. W. Wilkins, and K. G. Wilson, Phys. Rev. B **21**, 1003 (1980).

¹⁰ R. Bulla, T. A. Costi, and T. Pruschke, Rev. Mod. Phys. **80**, 395 (2008).

¹¹ A. M. Tsvelick and P. B. Wiegmann, Adv. Phys. **32**, 453 (1983).

¹² R. Hedden, V. Meden, T. Pruschke, and K. Schönhammer, J. Phys.: Condens. Matter **16**, 5279 (2004).

¹³ C. Karrasch, R. Hedden, R. Peters, T. Pruschke, K. Schönhammer, and V. Meden, J. Phys.: Condens. Matter **20**, 345205 (2008).

¹⁴ L. Bartosch, H. Freire, J. J. R. Cardenas, and P. Kopietz, J. Phys.: Condens. Matter **21**, 305602 (2009).

¹⁵ A. Isidori, D. Roosen, L. Bartosch, W. Hofstetter, and P. Kopietz, Phys. Rev. B **81**, 235120 (2010).

¹⁶ H. Freire and E. Corrêa, J. Low Temp. Phys. **166**, 192 (2012).

¹⁷ M. Kinza, J. Ortloff, J. Bauer, and C. Honerkamp, Phys. Rev. B **87**, 035111 (2013).

¹⁸ S. Streib, A. Isidori, and P. Kopietz, Phys. Rev. B **87**, 201107(R) (2013).

¹⁹ A. C. Hewson, J. Phys.: Condens. Matter **13**, 10011 (2001).

²⁰ A. C. Hewson, J. Phys.: Condens. Matter **18**, 1815 (2006).

²¹ K. Edwards and A. C. Hewson, J. Phys.: Condens. Matter **23**, 045601 (2011).

²² P. W. Anderson, J. Phys. C **3**, 2436 (1970).

²³ S. Kehrein, *The Flow Equation Approach to Many-Particle Systems*, Springer Tracts in Modern Physics, Vol. 217 (Springer, Berlin, 2006).

²⁴ E. Vogel, *Flussgleichungen für das Kondo-modell* (Dissertation, Heidelberg, 2005).

²⁵ W. Hofstetter and S. Kehrein, Phys. Rev. B **63**, 140402 (2001).

²⁶ D. Lobaskin and S. Kehrein, Phys. Rev. B **71**, 193303 (2005).

²⁷ C. Slezak, S. Kehrein, T. Pruschke, and M. Jarrell, Phys. Rev. B **67**, 184408 (2003).

²⁸ S. K. Kehrein and A. Mielke, J. Phys. A: Math. Gen. **27**, 4259 (1994).

²⁹ S. K. Kehrein and A. Mielke, J. Phys. A: Math. Gen. **27**, 5705 (1994).

³⁰ S. K. Kehrein and A. Mielke, Ann. of Phys. **252**, 1 (1996).

- ³¹ T. Stauber and F. Guinea, Phys. Rev. B **69**, 035301 (2004).
³² M. Zapalska and T. Domaníski, , arxiv:1402.1291 (2014).
³³ F. J. Wegner, Ann. Physik **3**, 77 (1994).
³⁴ S. D. Glazek and K. G. Wilson, Phys. Rev. D **48**, 5863 (1993).
³⁵ S. D. Glazek and K. G. Wilson, Phys. Rev. D **49**, 4214 (1994).
³⁶ F. Wegner, J. Phys. A: Math. Gen. **39**, 8221 (2006).
³⁷ S. Duffe and G. S. Uhrig, Eur. Phys. J. B **84**, 475 (2011).
³⁸ T. Fischer, S. Duffe, and G. S. Uhrig, New J. Phys. **10**, 033048 (2010).
³⁹ T. Fischer, S. Duffe, and G. S. Uhrig, Europhys. Lett. **96**, 47001 (2011).
⁴⁰ S. A. Hamerla, S. Duffe, and G. S. Uhrig, Phys. Rev. B **82**, 235117 (2010).
⁴¹ G. S. Uhrig and B. Normand, Phys. Rev. B **58**, 14705(R) (1998).
⁴² C. Knetter and G. S. Uhrig, Eur. Phys. J. B **13**, 209 (2000).
⁴³ H. Krull, N. A. Drescher, and G. S. Uhrig, Phys. Rev. B **86**, 125113 (2012).
⁴⁴ H.-Y. Yang and K. P. Schmidt, Europhys. Lett. **94**, 17004 (2011).
⁴⁵ A. Mielke, Eur. Phys. J. B **5**, 605 (1998).
⁴⁶ C. Knetter, K. P. Schmidt, and G. S. Uhrig, J. Phys. A: Math. Gen. **36**, 7889 (2003).
⁴⁷ A. Reischl, E. Müller-Hartmann, and G. S. Uhrig, Phys. Rev. B **70**, 245124 (2004).
⁴⁸ J. R. Schrieffer and P. A. Wolff, Phys. Rev. **149**, 491 (1966).

Appendix A: Adapted operator basis for the Kondo and Anderson impurity model

We consider the Hamiltonian from Eq. (26)

$$\begin{aligned}
 H_{\text{r}} = & \sum_{\sigma} \epsilon_r \left(c_{r\sigma}^{\dagger} c_{r\sigma} - c_{\bar{r}\sigma}^{\dagger} c_{\bar{r}\sigma} \right) \\
 & + J_{rr} \sum_{\mu} \sum_{\alpha, \beta} \sigma_{\alpha\beta}^{\mu} S_I^{\mu} \left(c_{r\alpha}^{\dagger} c_{r\beta} + c_{\bar{r}\alpha}^{\dagger} c_{\bar{r}\beta} \right) \quad (\text{A1})
 \end{aligned}$$

and its basis states. In the calculations presented in the main text we truncate basis states that are lying higher in energy than the triplet states. All basis states are shown below in the Tables II, III IV, V, and VI. The eigenstates are sorted by the number of fermions besides the impurity spin in the levels occurring in the Hamiltonian (A1). The arrow in the middle entry of the ket stands for the state of the impurity. The arrow to the left for the state of the particle state at $\epsilon_r > 0$; the arrow to the left for the state of the hole state at $-\epsilon_r < 0$. In addition, the total spin S and the total z-component S^z are given for the states. The column ‘used’ indicates whether or not the state is considered in our calculations.

states	energy ϵ_i	S	S^z	used
$ a_1\rangle = 0, \uparrow, 0\rangle$	$\epsilon_{a_1} = 0$	$\frac{1}{2}$	$+\frac{1}{2}$	no
$ a_2\rangle = 0, \downarrow, 0\rangle$	$\epsilon_{a_2} = 0$	$\frac{1}{2}$	$-\frac{1}{2}$	no

TABLE II. States with zero fermion besides the impurity spin

states	ϵ_i	S	S^z	used
$ s^-\rangle = \frac{1}{\sqrt{2}}(0, \uparrow, \downarrow\rangle - 0, \downarrow, \uparrow\rangle)$	$-\frac{3J_{rr}}{2} - \epsilon_r$	0	0	yes
$ t_1^-\rangle = 0, \uparrow, \uparrow\rangle$	$\frac{J_{rr}}{2} - \epsilon_r$	1	+1	yes
$ t_2^-\rangle = \frac{1}{\sqrt{2}}(0, \uparrow, \downarrow\rangle + 0, \downarrow, \uparrow\rangle)$	$\frac{J_{rr}}{2} - \epsilon_r$	1	0	yes
$ t_3^-\rangle = 0, \downarrow, \downarrow\rangle$	$\frac{J_{rr}}{2} - \epsilon_r$	1	-1	yes
$ a_3\rangle = \frac{1}{\sqrt{2}}(\uparrow, \downarrow, 0\rangle - \downarrow, \uparrow, 0\rangle)$	$-\frac{3J_{rr}}{2} + \epsilon_r$	0	0	no
$ a_4\rangle = \downarrow, \downarrow, 0\rangle$	$\frac{J_{rr}}{2} + \epsilon_r$	1	-1	no
$ a_5\rangle = \frac{1}{\sqrt{2}}(\uparrow, \downarrow, 0\rangle + \downarrow, \uparrow, 0\rangle)$	$\frac{J_{rr}}{2} + \epsilon_r$	1	+1	no
$ a_6\rangle = \uparrow, \uparrow, 0\rangle$	$\frac{J_{rr}}{2} + \epsilon_r$	1	+1	no

TABLE III. States with one fermion besides the impurity spin

states	ϵ_i	S	S^z	used
$ \text{FS}, \uparrow\rangle = 0, \uparrow, \uparrow\downarrow\rangle$	$-2\epsilon_r$	$\frac{1}{2}$	$+\frac{1}{2}$	yes
$ \text{FS}, \downarrow\rangle = 0, \downarrow, \uparrow\downarrow\rangle$	$-2\epsilon_r$	$\frac{1}{2}$	$-\frac{1}{2}$	yes
$ \uparrow\rangle = \frac{1}{\sqrt{6}}[\uparrow, \uparrow, \downarrow\rangle - 2 \uparrow, \downarrow, \uparrow\rangle + \downarrow, \uparrow, \uparrow\rangle]$	$-2J_{rr}$	$\frac{1}{2}$	$+\frac{1}{2}$	yes
$ \downarrow\rangle = \frac{1}{\sqrt{6}}[\downarrow, \downarrow, \uparrow\rangle - 2 \downarrow, \uparrow, \downarrow\rangle + \uparrow, \downarrow, \downarrow\rangle]$	$-2J_{rr}$	$\frac{1}{2}$	$-\frac{1}{2}$	yes
$ a_{11}\rangle = \frac{1}{\sqrt{2}}[\uparrow, \uparrow, \downarrow\rangle - \downarrow, \uparrow, \uparrow\rangle]$	0	$\frac{1}{2}$	$+\frac{1}{2}$	no
$ a_{12}\rangle = \frac{1}{\sqrt{2}}[\downarrow, \downarrow, \uparrow\rangle - \uparrow, \downarrow, \downarrow\rangle]$	0	$\frac{1}{2}$	$-\frac{1}{2}$	no
$ a_{13}\rangle = \frac{1}{\sqrt{3}}[\uparrow, \uparrow, \downarrow\rangle + \uparrow, \downarrow, \uparrow\rangle + \downarrow, \uparrow, \uparrow\rangle]$	J_{rr}	$\frac{3}{2}$	$+\frac{1}{2}$	no
$ a_{14}\rangle = \frac{1}{\sqrt{3}}[\downarrow, \downarrow, \uparrow\rangle + \downarrow, \uparrow, \downarrow\rangle + \uparrow, \downarrow, \downarrow\rangle]$	J_{rr}	$\frac{3}{2}$	$-\frac{1}{2}$	no
$ a_{15}\rangle = \uparrow, \uparrow, \uparrow\rangle$	J_{rr}	$\frac{3}{2}$	$+\frac{3}{2}$	no
$ a_{16}\rangle = \downarrow, \downarrow, \downarrow\rangle$	J_{rr}	$\frac{3}{2}$	$-\frac{3}{2}$	no
$ a_{17}\rangle = \uparrow\downarrow, \uparrow, 0\rangle$	$2\epsilon_r$	$\frac{1}{2}$	$+\frac{1}{2}$	no
$ a_{18}\rangle = \uparrow\downarrow, \downarrow, 0\rangle$	$2\epsilon_r$	$\frac{1}{2}$	$-\frac{1}{2}$	no

TABLE IV. States with two fermions besides the impurity spin

states	ϵ_i	S	S^z	used
$ s^+\rangle = \frac{1}{\sqrt{2}}(\downarrow, \uparrow, \uparrow\downarrow\rangle - \uparrow, \downarrow, \uparrow\downarrow\rangle)$	$-\frac{3J_{rr}}{2} - \epsilon_r$	0	0	yes
$ t_1^+\rangle = \uparrow, \uparrow, \uparrow\downarrow\rangle$	$\frac{J_{rr}}{2} - \epsilon_r$	1	+1	yes
$ t_2^+\rangle = \frac{1}{\sqrt{2}}(\downarrow, \uparrow, \uparrow\downarrow\rangle + \uparrow, \downarrow, \uparrow\downarrow\rangle)$	$\frac{J_{rr}}{2} - \epsilon_r$	1	0	yes
$ t_3^+\rangle = \downarrow, \downarrow, \uparrow\downarrow\rangle$	$\frac{J_{rr}}{2} - \epsilon_r$	1	-1	yes
$ a_7\rangle = \frac{1}{\sqrt{2}}(\uparrow\downarrow, \downarrow, \uparrow\rangle - \uparrow\downarrow, \uparrow, \downarrow\rangle)$	$-\frac{3J_{rr}}{2} + \epsilon_r$	0	0	no
$ a_8\rangle = \uparrow\downarrow, \uparrow, \uparrow\rangle$	$\frac{J_{rr}}{2} + \epsilon_r$	1	+1	no
$ a_9\rangle = \uparrow\downarrow, \downarrow, \downarrow\rangle$	$\frac{J_{rr}}{2} + \epsilon_r$	1	-1	no
$ a_{10}\rangle = \frac{1}{\sqrt{2}}(\uparrow\downarrow, \downarrow, \uparrow\rangle + \uparrow\downarrow, \uparrow, \downarrow\rangle)$	$\frac{J_{rr}}{2} + \epsilon_r$	1	0	no

TABLE V. States with three fermions besides the impurity spin

states	ϵ_i	S	S^z	used
$ 4, \uparrow\rangle = \uparrow\downarrow, \uparrow, \uparrow\downarrow\rangle$	0	$\frac{1}{2}$	$+\frac{1}{2}$	no
$ 4, \downarrow\rangle = \uparrow\downarrow, \downarrow, \uparrow\downarrow\rangle$	0	$\frac{1}{2}$	$-\frac{1}{2}$	no

TABLE VI. States with four fermions besides the impurity spin